Naval Research Laboratory
Monterey, CA 93943-5502

A Study of Westerly Wind Bursts Preceding the 1991-1992 El Niño

Patricia A. Phoebus

Data Assimilation Section
Marine Meteorology Division

John C. Kindle

Coupled Dynamic Processes Section
Oceanography Division

July 27, 1994

1. AGENCY USE ONLY (Leave Blank)	2. REPORT DATE July 1994	3. REPORT TYPE AND DATES COVERED Final

4. TITLE AND SUBTITLE A Study of Westerly Wind Bursts Preceding the 1991-1992 El Niño	5. FUNDING NUMBERS PE 0602704N PN 7W0513 AN DN153154

6. AUTHOR(S)

Patricia A. Phoebus[1] and John C. Kindle[2]

7. PERFORMING ORGANIZATION NAME(S) AND ADDRESS(ES) Naval Research Laboratory:[1]Marine Meteorology Division, Monterey, CA 93943-5502;and [2]Oceanography Division,Stennis Space Center, MS 39529-5004	8. PERFORMING ORGANIZATION REPORT NUMBER NRL/FR/7531--94-9450

9. SPONSORING/MONITORING AGENCY NAME(S) AND ADDRESS(ES) Office of Naval Research 800 North Quincy Street Arlington, VA 22217-5660	10. SPONSORING/MONITORING AGENCY REPORT NUMBER

11. SUPPLEMENTARY NOTES

12a. DISTRIBUTION/AVAILABILITY STATEMENT Approved for public release; distribution unlimited.	12b. DISTRIBUTION CODE

13. ABSTRACT (Maximum 200 words)

Anomalous westerly wind events in the western equatorial Pacific are of interest because of their potential to generate equatorially trapped ocean Kelvin waves that may be related to the development or enhancement of the El Niño. While a number of ideas have been proposed about the nature and origin of the equatorial westerlies, detection and description of these events is hindered by the lack of observational data in the area of interest (3°S-3°N, 130°E-180°E). Under such circumstances, the best tool for obtaining a realistic representation of the atmosphere is a four-dimensional global data assimilation system,which continually updates a short-term model forecast using synoptic data to produce meteorological fields that are consistent with known dynamical and physical relationships. Using low-level wind fields from the U. S. Navy's operational global analysis/forecast system for the period October 1990-February 1992, we observed a clear association between significant westerly wind events and tropical cyclone development. In general, there is an eastward and equatorward shift in cyclone activity that is associated with the concentration of westerlies along the equator in the western and central Pacific. The strongest westerlies are associated with the development of dual-hemisphere cyclone pairs, and these events preceded the maximum warming in the eastern Pacific by a couple of months, thus supporting the hypothesis for ocean Kelvin wave contributions to the El Niño. Similar patterns in tropical cyclone activity are observed during other years marking the beginning of the El Niño.

14. SUBJECT TERMS El Niño Southern oscillation ENSO Westerly wind bursts NOGAPS	15. NUMBER OF PAGES 59
	16. PRICE CODE

17. SECURITY CLASSIFICATION OF REPORT UNCLASSIFIED	18. SECURITY CLASSIFICATION OF THIS PAGE UNCLASSIFIED	19. SECURITY CLASSIFICATION OF ABSTRACT UNCLASSIFIED	20. LIMITATION OF ABSTRACT Same as report

CONTENTS

A STUDY OF WESTERLY WIND BURSTS PRECEDING THE 1991-1992 EL NIÑO

1 INTRODUCTION

Perhaps no other phenomenon that occurs in the atmosphere/ocean system has as far-reaching an impact as the El Niño-Southern Oscillation (ENSO). The warm cycle of the ENSO manifests itself not only in changes to the sea surface temperature and precipitation patterns in the tropical Pacific (Rasmusson and Carpenter, 1982), but it also has been connected to anomalous weather patterns worldwide, including floods in the southern United States, droughts in Australia, Indonesia, and southeastern Africa (Ropelewski and Halpert, 1987), disruption of the Indian monsoon, decreases in Atlantic hurricane activity (Gray, 1984), and fewer South Pacific typhoons (Solow and Nicholls, 1990). Notable changes also have been observed in fish and bird populations in much of the eastern Pacific (Barber and Chavez, 1983). As such, ENSO has captured the attention of scientists across a broad range of disciplines, including marine biologists, physical and dynamical oceanographers, climatologists, atmospheric and oceanographic modelers, and synoptic meteorologists. Each of these groups contributes unique pieces to the ENSO puzzle, as the scientific community attempts to construct a cohesive explanation of this phenomenon.

Both the historical and current states of knowledge related to ENSO have been recently compiled by Philander (1990). While it is well accepted that ENSO involves complex interactions between the ocean and the atmosphere, the exact nature of those interactions is still in question. Clearly, the tropical ocean responds very rapidly to changes in atmospheric wind forcing, while the atmosphere responds to changes in the sea surface temperature pattern. But the mechanisms that produce the apparent switch between the cold and warm cycles of the Southern Oscillation (SO) and the quasi-periodicity of these events are not well understood and are still being discussed (see, for example, Graham and White, 1988; Masumoto and Yamagata, 1991; Wakata and Sarachik, 1991; Gray et al., 1992).

Much of the recent attention has focused on anomalous westerly wind events in the western equatorial Pacific. These highly energetic, short-lived events, often called westerly wind bursts, can trigger equatorially trapped ocean Kelvin waves that transverse the Pacific Ocean to the coast of South America. These downwelling waves inhibit the upwelling of colder, deeper water such as that normally observed off the coast of South America, and thus may be responsible in part for the dramatic changes in sea-surface temperature (SST) and sea-surface height (SSH) that are observed in the eastern and central Pacific during the El Niño. Westerly wind bursts may also generate anomalous easterly currents that advect warm surface waters, pooled in the western Pacific by the prevailing easterly trade winds, eastward. These hypotheses have received support from both observational and modeling studies (McPhaden et al., 1988; Giese and Harrison, 1990).

However, there are typically very few actual observations made in the tropics, where ENSO manifests itself. It is fair to say that perhaps no other phenomenon has been studied more with less data. Much of what has been learned has been determined either from model simulations of the ocean and atmosphere (McCreary and Anderson, 1991), statistical descriptions of the mean anomalous patterns (Rasmusson and

Carpenter, 1982), or studies from time series at isolated data points (Luther et al., 1983; Morrissey, 1990; Chu et al., 1991; Harrison and Giese, 1991). Coupled ocean/atmosphere model simulations have been successful in isolating low-frequency oscillations that may be associated with ENSO. But the atmospheric models used in most modeling studies are purposefully oversimplified, and thus they cannot simulate the impact of higher frequency forcing mechanisms that may play an important role in the irregular nature of the oscillation (Philander, 1990). Statistical studies suffer from the same limitation, in that the high-frequency events can be disguised, damped, or eliminated by the averaging process. Finally, while time series of ship and island wind reports may help determine the strength, frequency, and duration of the westerly bursts, they provide only limited information about the spatial extent of the events.

Unfortunately, given the lack of observational data in the tropical Pacific, regular detection of the anomalous westerly wind events is difficult. Although recently deployed buoys in the equatorial Pacific have provided a new source of additional observations, it still will be difficult to produce a coherent image of a westerly wind burst from this limited data set (Mangum et al., 1992). Under such circumstances, the best tool for obtaining a realistic representation of the atmosphere is a four-dimensional global data assimilation system, which continually updates a reasonably accurate short-term model forecast using newly obtained data to produce meteorological fields that are consistent with known dynamical and physical relationships. The model forecast carries forward information from past observations, while the analysis blends this information with data from new observations. The range of influence for a particular observation within this environment is controlled by a set of mathematical relationships.

In this study, we use an operational global atmospheric data assimilation system, coupled to a global ocean data assimilation system, to look at the synoptic-scale atmospheric events that may affect the evolution of the tropical ocean. Both analysis/forecast systems make use of all the available oceanographic and atmospheric data in real-time. While the tropics is one of the most difficult areas to model successfully, improvements continue to be made due to increased resolution, improved physical parameterizations, new data analysis techniques, and better data quality control. The U. S. Navy's research and development efforts in support of the Joint Typhoon Warning Center (JTWC) in Guam have resulted in an operational global atmospheric data assimilation and prediction system that is particularly active in the tropics. The last few years, this system has been accurately analyzing and forecasting westerly wind bursts associated with tropical circulations in the western Pacific. From the model output, we can observe the progression of these events over time and determine the spatial scales associated with each burst.

This report concentrates on the westerly wind events that occurred in the western tropical Pacific from the fall of 1990 through the winter season of 1991-1992 (the period leading up to the most recent El Niño), while a follow-on study (Kindle and Phoebus, 1994) focuses on the ocean response to that wind forcing. We are particularly interested in the association between westerly wind bursts and tropical cyclones. Several studies have noted that strong westerly winds along the equator are associated with the development of tropical cyclone couplets in the western Pacific (Keen, 1982; Ogura and Chin, 1987; Lander, 1989), and both Keen (1988) and Ramage (1986) have proposed that these storms play a key role in the onset of El Niño. On the other hand, Harrison and Giese (1991) found only a 40% association between westerly wind bursts and named tropical storms over a 25-year period. Their study was limited, however, in that only isolated observations in a limited area were utilized. By using the spatially coherent fields from an operational data analysis/forecast model system, the association between tropical cyclones and westerly wind bursts can be studied in more detail.

Since the target audience for this report includes the oceanographic community, we first describe the operational atmospheric database and discuss the characteristics of the observations typically available in the tropical Pacific in Section 2. Section 3 describes atmospheric data assimilation techniques and provides background information on the various components and relative skill of the Navy Operational Global

Atmospheric Prediction System (NOGAPS). Readers who are already familiar with these topics may wish to skip to Section 4, where we present the most notable westerly wind bursts preceding the 1991-1992 El Niño and discuss their relationships to the western Pacific tropical cyclones. While we do not propose to fit all the pieces together, in Section 5 we attempt to put these events into perspective and relate our results to other ENSO research; Section 6 summarizes the study.

2   THE GLOBAL DATABASE

With a few exceptions, most of the world's operational forecast centers have access to the same observational data. Atmospheric soundings are taken by rawinsondes, pilot balloons, and the polar-orbiting satellites. Single-level measurements of the upper atmosphere are available from aircraft and the geostationary satellites, while the marine surface layer is sampled by satellites, ships, moored and drifting buoys, and coastal marine stations.

The majority of the conventional observations are concentrated in the northern mid-latitudes. Approximately 90% of the 700 or so radiosonde stations are in the Northern Hemisphere, primarily on the continents. The pilot balloon stations are smaller in number (100-200), but they are more evenly distributed between the hemispheres and nearly half of the stations are in the tropics. Moored buoys and coastal marine stations are predominantly along coastlines, while over the open ocean, aircraft and ship reports are clustered along the major flight paths and shipping lanes. Drifting buoys are still too few in number to provide adequate global coverage of the marine surface layer.

Thus, remotely sensed data can be an important supplement to the conventional database. Temperature soundings are derived from radiance measurements made by four polar-orbiting satellites, two from the National Oceanographic and Atmospheric Administration (NOAA) and two from the Defense Meteorological Satellite Program (DMSP). The satellite soundings are used at all levels over the oceans, but because their accuracy is considerably less than that of the rawinsondes, satellite sounding data are used only in the stratosphere over land, a practice common to most all the operational centers. However, the U. S. Navy's Fleet Numerical Meteorology and Oceanography Center (FNMOC) is the only center using the DMSP soundings in addition to the NOAA soundings.

Single-level measurements of the upper atmosphere include wind reports from aircraft (both automated and pilot reports) and cloud-tracked wind information derived from the geostationary satellites of the United States, Europe, and Japan. The aircraft data are concentrated at cruising altitudes (300-200 mb) along major flight routes, while the cloud-tracked winds are vertically clustered from 925-850 mb at low levels and 300-200 mb at higher levels. Because of the limited viewing area of the geostationary satellites, most of the satellite-derived wind observations are between 50°N and 50°S, with roughly half in the tropics. The cloud-tracked wind reports are probably the least accurate of the various wind observations, mainly because of problems associated with correctly assigning the cloud to a specific height in areas where no supplemental information is available about the detailed vertical structure of the moisture field.

Conventional surface observations are made by land stations, moored and drifting buoys, coastal marine stations, and ships. Except for the recent addition of wind reports from the tropical Pacific islands to NOGAPS (Phoebus and Goerss, 1992), no surface wind reports over land are used in the analysis. Terrain effects and shallow radiation inversions often result in surface wind reports that are not representative of the free atmosphere. This problem is avoided somewhat in the tropics by using only island wind observations with speeds that exceed 3.5 m/s, which likely indicates a well-mixed boundary layer. There are about 100 islands in the tropical Pacific that report surface wind and pressure, but not all of these stations report routinely. Ships, coastal marine stations, and moored buoys provide both sea-level

pressure and wind observations. However, 90% of these observations are in the Northern Hemisphere. Many of the drifting buoys provide sea-level pressure observations but most do not have wind sensors, so their usefulness in defining the tropical marine atmosphere is limited.

A new source of surface wind data, first utilized in an operational data assimilation system by the U. S. Navy, is the Special Sensor Microwave/Imager (SSM/I) flown on the DMSP satellites. FNMOC has been evaluating and assimilating SSM/I surface wind speed observations into the global analysis/forecast system since September, 1990 and was the only forecast center using these data operationally prior to May, 1993. Because the 25-km resolution of the SSM/I data represents much finer scales than those resolved by NOGAPS, the SSM/I wind speeds are sub-sampled and averaged to 200-km resolution. Then, wind directions are assigned using the 10-m wind fields produced by the forecast model from a preliminary analysis of the conventional data (Phoebus and Goerss, 1992). The near global coverage of the SSM/I winds provides an important addition to the ship and buoy reports, particularly because of the U. S. Navy's reliance on accurate low-level marine analyses and forecasts.

It is not unusual for the operational centers to supplement the global database by creating synthetic observations for specific applications. For example, the Australian Bureau of Meteorology subjectively derives estimates of sea level pressure in the Southern Hemisphere from satellite imagery. These observations are provided to and used by the other operational centers. At FNMOC, they are excluded north of 20°S. Locally, FNMOC personnel generate synthetic observations of sea level pressure and surface winds in the vicinity of oceanic extra-tropical cyclones (Goerss, 1989). Typically, such observations are created in data-sparse areas like the North Pacific, in situations where satellite imagery indicates that the cyclone is deeper than its model depiction.

Finally, of particular importance to this paper, synthetic wind soundings and 1000 mb height observations are automatically generated in the vicinity of tropical storms (Goerss et al., 1991). The soundings are the sum of two components: one from the large-scale environmental flow obtained by spectrally truncating the NOGAPS model wind field, and the other from a symmetric Rankine vortex in gradient balance centered at the storm's location. The structure of the Rankine vortex is controlled by the storm's maximum wind speed and the radius of maximum winds (Phoebus and Goerss, 1992). The information required to define the Rankine vortex is taken directly from the warning messages issued by the Joint Typhoon Warning Center (JTWC), Guam, and the National Hurricane Center, Miami, once the cyclones reach tropical storm strength. Since these locally created synthetic observations are specifically related to NOGAPS performance, they are not distributed to the other centers. Although other operational centers are interested in this technique, the insertion of tropical storms using synthetic soundings derived from operational warning messages was unique to the U. S. Navy during the time of this study.

Having described the global database, we can now focus on the observations typically available in the tropical western Pacific. We are primarily interested in the westerly wind events that occur within plus or minus 3 degrees of the equator between Indonesia and the date line (130-180°E), since these are the events that produce the largest ocean response (Giese and Harrison, 1991). There are no radiosonde stations located within this region, so the only sounding data available are from the polar-orbiting satellites, which provide temperature data that can be converted to geopotential thickness observations. However, since geostrophy is less applicable in the tropics, we are more interested in wind observations. We can disregard drifting buoys since they do not, for the most part, provide wind information. Occasion: wind reports are available from ships of opportunity, but such observations are infrequent in the area of interest. There are a few islands in this area, but none west of 165°E. Thus if the westerlies do not extend far to the east, they will not be detected in the island wind observations. As a result of the TOGA (Tropical Ocean Global Atmosphere) program, NOAA has deployed lines of moored buoys perpendicular to the equator at 165°E and more recently at 156°E (July, 1991) and other locations in the western

tropical Pacific. However, receipt of the Tropical Atmosphere-Ocean (TAO) buoy data via the Global Telecommunication System (GTS) was limited and erratic during the period of this study.

In contrast to what we don't have, what we do have are low-level cloud-tracked winds from the Japanese. These observations are fairly numerous and can be a valuable source of information for analyzing the lower atmosphere, if they happen to be in or near the area of interest. Also, at the time of this study, the U. S. Navy was assimilating the SSM/I surface wind speed data and the synthetic tropical cyclone observations. While the SSM/I data do not provide wind direction, they may assist in accurately modeling the strength of the westerly wind events. And if indeed these events are associated with tropical cylone activity, the more accurate depiction of tropical cyclones that results from the insertion of the synthetic tropical soundings could play a key role in capturing the westerly wind events.

Although the narrowly defined area of interest is a data-sparse zone, the region south and west of this area contains a wealth of information and there are numerous island observations to the north and east. We argue that a global data assimilation system can effectively utilize this information to provide a realistic estimate of the wind fields over the data-sparse region. Furthermore, the four-dimensional model depiction of the wind field may aid in understanding the dynamical and physical processes associated with these westerly wind events.

3   THE GLOBAL DATA ASSIMILATION SYSTEM

The U.S. Navy's operational global atmospheric prediction system (NOGAPS) consists of four components: data preprocessing and quality control, the data analysis, the initialization of the analyzed fields, and the model forecast. This analysis/forecast system is run with a 6-h update cycle, where the 6-h model forecast provides the first-guess for the next data analysis, and the analysis updates the first-guess using new observations to provide the initial conditions for the next model forecast. Each new analysis includes all observations within plus or minus 3 h of the synoptic analysis time, regardless of the time the analysis is actually performed. For example, the assimilation cycle includes a 00Z and 12Z re-analysis at 9 h after the synoptic time, thereby allowing late-arriving observations to influence the first-guess fields used by the next analysis (Goerss and Phoebus, 1992). The various components of NOGAPS are described in detail elsewhere, so only the highlights will be reiterated here.

3.1   Quality Control

The data preprocessing and quality control performed prior to the analysis execute several different quality checks on each observed value (Baker, 1992). Depending on the data type, these tests may include checks for location, timeliness, climatological ranges of values, and vertical consistency. Some values may be recomputed, where possible, and some radiosonde observations are corrected for known biases. Each observation is then flagged to indicate whether it should be rejected, subjected to further checking, or accepted as is.

All observations flagged for further checking are subjected to a gross-error check within the analysis to ensure that they do not vary greatly from the first-guess. This gross-error check is very lenient for the most part, with the particular tolerance given an observation dependent on the data type and its location (Goerss and Phoebus, 1993). Data may be rejected outright at this stage, or flagged for further checking. The final quality check is performed as an integral part of the analysis process and requires that surrounding observations corroborate each suspicious observation, or the suspect value is ignored by the analysis. In all, the number of observations rejected by the analysis is small: approximately 1% of the surface data, 2% of the observed values from rawinsondes, 4-5% of the aircraft reports, and 7% of the

layer thicknesses from satellite soundings, with a high of 15-20% for the cloud-tracked winds. Each piece of information within a sounding is quality checked and accepted or rejected individually. However, if one wind component is flagged or rejected, its associated component must be treated likewise.

3.2 Analysis

The data analysis uses a multivariate optimum interpolation (MVOI) technique patterned after that of the European Centre for Medium Range Weather Forecasts (ECMWF; Lorenc, 1981) to produce three-dimensional gridded fields of geopotential height and the zonal and meridional wind components (u and v, respectively). The analysis is performed on a 1.5 degree Gaussian grid at the 16 standard pressure levels from 1000-10 mb. The MVOI ideally will make only small changes to the model-predicted fields. These adjustments are computed from the observation increments (the observation/prediction differences), which are formed by interpolating the gridded first-guess fields to the observation locations and subtracting the interpolated values from the observed values of each parameter. The observation increments are more homogeneous than the observations themselves, so these are the values that are actually analyzed. The MVOI is an incremental analysis, where the analyzed increments at the grid locations are added to the first-guess values to produce the new analysis.

Unlike simpler methodologies that merely average the observations within some radius of influence about each grid point, the MVOI determines how the observations are combined in a more rigorous fashion, by recognizing that both the observed values and the model-predicted values are inexact. By requiring that that the analysis error variance be minimized when computed over a statistically significant number of cases, an expression for the weights of the observation increments is derived. The weight a particular increment receives relative to the analyzed value at a particular grid point is a function of the observation errors of the data, specified by data type; the error in the first-guess at the grid point location (prediction error); and the prediction error correlations between the various observation and grid point locations. These statistics can be estimated fairly accurately from historical databases of observation minus first-guess increments (Goerss and Phoebus, 1993).

In a three-dimensional multivariate system, the analyzed variables are assumed to be geostrophically related. Thus, the horizontal and vertical error correlation functions must account for the relationships between all possible variable combinations for multiple levels in the atmosphere. That way, observed wind increments will affect the height analysis as well as the wind analysis, while a height or thickness increment will modify the wind field in a manner consistent with the changes made to the mass field. However, in the tropics, the geostrophic constraint is relaxed, and mass observations have a much smaller impact on the resulting wind analysis.

3.3 Initialization

While the set of prediction error correlation functions ensures that the analyzed increments in the extratropics are in geostropic balance, there is no assurance that the full analyzed fields are in appropriate balance for the forecast model,which is why the latter must be initialized before they are used by the model. The removal of inconsistencies between the analyzed fields and the internal dynamics of the model is accomplished by a nonlinear normal mode initialization (NNMI; Machenhauer, 1977). The normal modes are derived from the adiabatic model equations linearized about a basic state at rest with horizontally uniform surface pressure and temperature fields. The modes describe the spectrally truncated fields of divergence, vorticity, and a form of the geopotential that combines the effects of both pressure and temperature variations (Hogan et al., 1991). The horizontal and vertical structures are determined separately as eigenvectors of the linearized system. There are 18 vertical modes, corresponding to the number of model levels.

The current operational NNMI initializes three vertical modes, the external and first two internal modes, using an iterative scheme. Two iterations of this scheme are performed, not including the calculations of the initial tendencies. A frequency cut-off is employed that restricts the subset of initialized modes to those with natural periods less than 24 hours. The vertical mode and frequency cut-off values were determined empirically and appear to eliminate most of the undesirable initial gravity waves without severely damaging the meteorologically significant divergent circulations. This latter point is especially crucial for preserving the character of certain tropical circulations.

3.4 Model Forecast

Once the synoptic data have been assimilated by the MVOI and the analyzed fields have been adjusted by the NNMI, these fields provide the initial conditions for the next model forecast. The model extrapolates from the current state of the atmosphere into the future by solving a set of diagnostic and prognostic equations that describe the dynamical and physical processes in the atmosphere. The particular forms of these equations and the associated physical parameterizations are given by Hogan and Rosmond (1991). The operational model run during the period of this study was a global spectral model with 79-wave triangular truncation (T79), which corresponds to a 1.5 degree Gaussian transform grid. The model equations are formulated in spherical coordinates horizontally, with a hybrid vertical coordinate that represents a slightly modified sigma-coordinate system, which varies from 1 at the terrain surface to 0 at the top of the model. There are 18 vertical levels from the surface to 10 mb, with five model layers concentrated within 200 mb of the surface to better resolve boundary layer processes, and four layers used above 100 mb to resolve the stratosphere.

The prognostic variables for motion are vorticity and divergence. The thermodynamic variable of the model is virtual potential temperature, which is altered with time through both advection and diabatic heating. The diabatic heating is the sum of the radiation, the latent heat release, and the horizontal and vertical diffusion processes. The moisture equation predicts the time rate of change of specific humidity as a function of advection and of the moistening term. The latter term accounts for turbulent and cumulus vertical mixing, the condensation-evaporation processes, and horizontal diffusion. The hydrostatic equation, mass continuity equation, and vertical motion equation complete the set of model equations.

The sea-surface temperatures that are used in the boundary layer parameterization are provided by an ocean data assimilation system (Clancy et al., 1990; Clancy et al., 1992) that is run in a 24-h update cycle with a mixed layer model. This system includes a three-dimensional ocean thermal analysis that uses optimum interpolation to blend temperature data from ships, buoys, satellites, and bathythermographs with model-predicted temperatures and climatological values. The mixed layer model extends from the surface to 400 m, and is forced with heat fluxes and surface wind stresses from the atmospheric model. The resulting temperature fields are available on a 1.25 grid. Operationally, the oceanic and atmospheric data assimilation systems are loosely coupled, that is, the ocean mixed layer model receives new forcing fields from NOGAPS every 3 hours, while the SST field remains fixed during a full 24-h atmospheric assimilation cycle.

The physical parameterizations within the NOGAPS model are both numerous and complex, and are key ingredients for successful data assimilation in the tropics. Therefore, the interested reader is referred to Hogan and Rosmond (1991) and Hogan and Brody (1993) for descriptions of how the diabatic processes are computed within the model. For the purposes of this report, we will simply state that the diabatic processes include gravity-wave drag, vertical fluxes, ground temperature and moisture, shallow convection, convective mixing, cumulus (including precipitation evaporation and a simple evaporative downdraft), large-scale precipitation, cloud fractions, longwave radiation (including ice emissivity), and shortwave radiation. All of these computations are performed on the Gaussian grid.

The spectral model was originally implemented in 1988 with a T47 resolution and a less sophisticated set of physical parameterizations. It was not until the incorporation of the more complete atmospheric physics package in March, 1989 that a marked improvement was seen in the tropics (Hogan and Rosmond, 1991). Shortly thereafter, in August, 1989, the model's resolution was increased to T79. This combination of changes resulted in a forecast model that was actively spinning up tropical circulations and forecasting their development and movement. Thus, the assimilation of synthetic tropical soundings was added to the analysis to better position the tropical storms in the model's initial state. It is important to note that without the model's skill in the tropics, the forced insertion of tropical circulations in the analysis would be ineffective, since the model might quickly dampen the initial circulation. But because the model is able to maintain these circulations throughout its forecast period, we now have a global data assimilation system whose tropical forecasting skill is comparable to or better than the currently accepted tropical forecasting aids (Fiorino et al., 1993a).

An example of early development of a tropical cyclone by NOGAPS is shown in Figure 1. The NOGAPS sea level pressure analysis valid at 00Z on November 20, 1990 (Fig. 1a) shows only a slight hint of the tropical depression that is located near 8°N, 147°E. The 72- and 120-h forecasts made from this analysis, however, clearly indicate that this depression will develop into a major tropical cyclone (Fig. 1b,c). The verifying positions of Tropical Storm Page and Typhoon Page are also shown on these figures. Even though no synthetic observations were ingested into this analysis/forecast series, the track errors in the 72-h and 120-h forecasts were around 500 km and 800 km, respectively. In Figure 1d-f, a similar series is shown, but for 3 days later. At the time of this analysis, Page was a tropical storm and synthetic soundings were being generated for the analysis. Even though a global model cannot actually respresent the true intensity of such storms, the analysis now has two closed isobars depicting the cyclone, and the drop in pressure throughout the forecast period is more dramatic than in the previous series. The 72-h and 120-h position errors are also reduced substantially, to where the 120-h position error is only around 350 km. The second series also shows the forecasted positions of Typhoon Owen to the east of Page. Although the position for Owen is not nearly as accurate, at least the model is beginning to depict this second storm.

3.5 Verification

While case studies such as those in Figure 1 provide some reference for determining model skill in specific situations, overall model skill is difficult to determine qualitatively. A statistic commonly used by the operational centers for skill comparisons is the 500-mb height anomaly correlation for the Northern Hemisphere midlatitudes (Rosmond, 1992). The anomaly correlation quantifies the ability of a data assimilation system to forecast departures from climatology. A value greater than 0.6 is generally accepted as the measure of a forecast that has some usefulness. The anomaly correlations in Figure 2 illustrate the general improvement in NOGAPS forecasts from 1987 through 1990. During this time, not only did the skill improve steadily for each forecast period, but at least a one-day gain was made. For example, the 48-h forecasts in 1990 were better overall than the 72-h forecasts were in 1987.

A recent comparison of anomaly correlations from NOGAPS to those computed for some of the other operational centers reveals only a small spread in the forecast statistics (Fig. 3). These values were computed using fields sent to FNMOC by the other operational centers, which are not necessarily the full-resolution fields produced operationally at each center. The fields distributed by the National Meteorological Center (NMC), the Japan Meteorological Agency (JMA), and FNMOC are 2.5 degree resolution, while ECMWF fields are 5.0 degree resolution. In actuality, the NOGAPS T79 model has a much coarser resolution than the T126 implemented at the NMC in March, 1991 and the T213 run at the ECMWF since September, 1991. The anomaly correlation for each center is computed in reference to
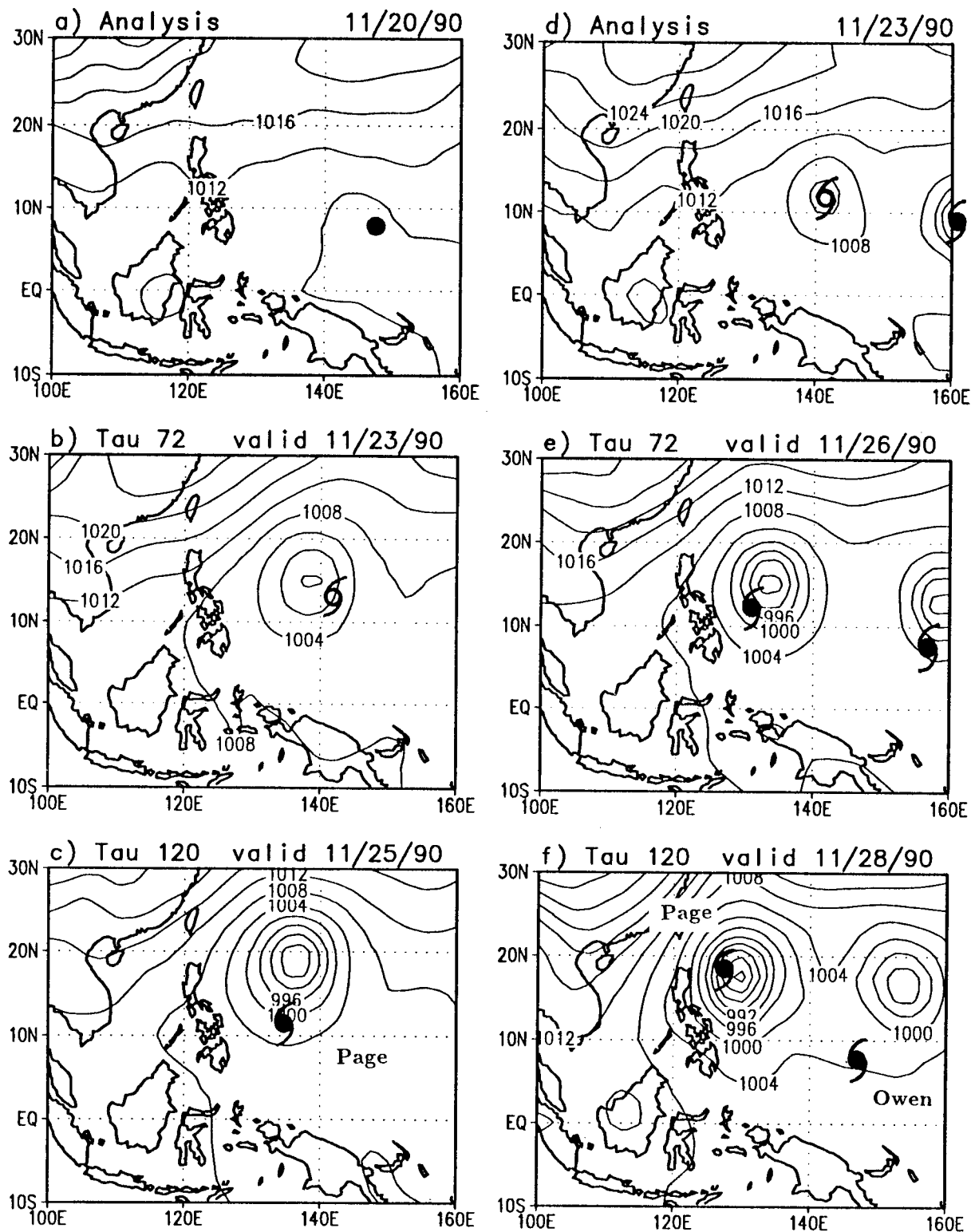
Fig. 1 — NOGAPS 00Z surface pressure analyses and forecasts with verifying positions of the tropical cyclones annotated. a) Analysis valid November 20, 1990. b) 72-h forecast valid November 23, 1990. c) 120-h forecast valid November 25, 1990. d) Analysis valid November 23, 1990. e) 72-h Forecast valid November 26, 1990. f) 120-h Forecast valid November 28, 1990.
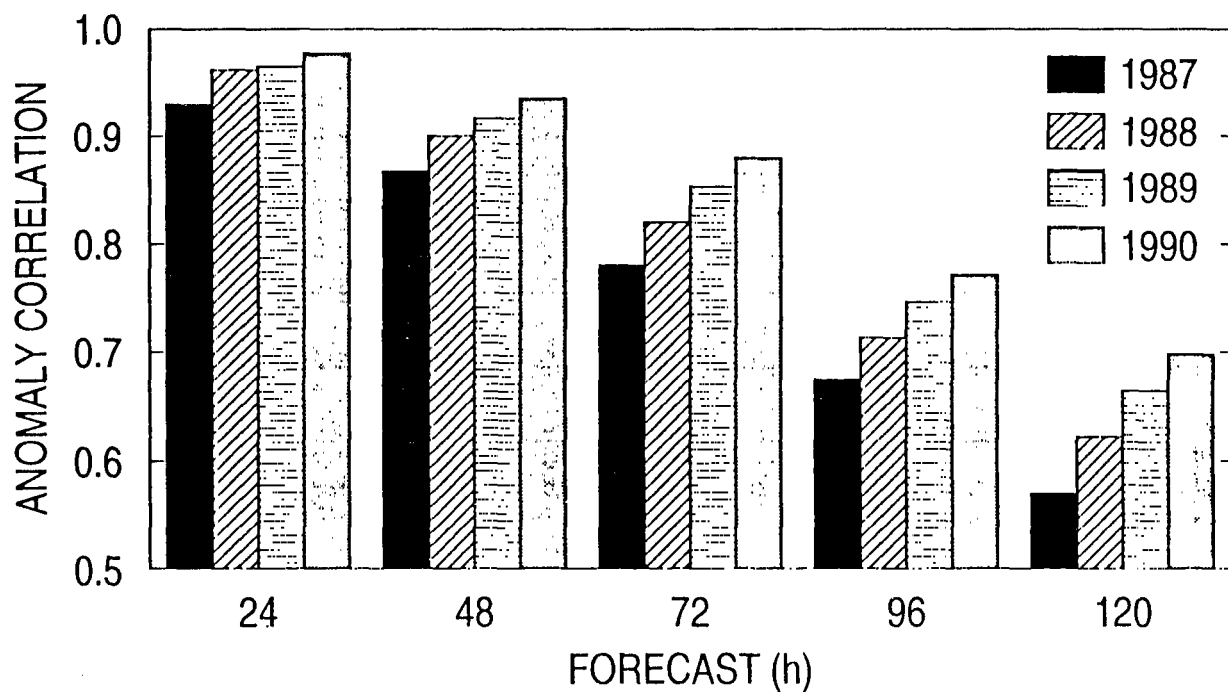
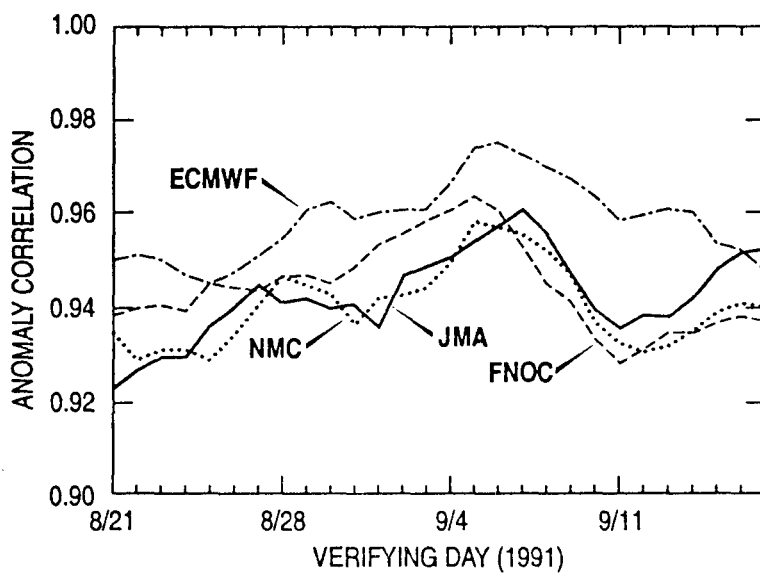Fig. 2 – NOGAPS mean annual anomaly correlations for the northern mid-latitudes (20° N-80° N)

Fig. 3 – Anomaly correlations for the 48-h 500-mb height forecast in the northern mid-latitudes from four different operational centers. The values are 5-day running means comparing forecast fields to self-analyses.

their own analysis, rather than in reference to the NOGAPS analysis. The results shown here were typical of the period, with ECMWF slightly ahead of the other centers and no clear standout for second place.

However, forecasting skill in the midlatitudes does not necessarily translate to skill in modeling the tropics, where the physical parameterizations of the model become even more critical. Furthermore, the problem of model verification is exacerbated due to the lack of sufficient observational data. Thus, we will assume that the skill of a data assimilation system in the tropics can be tied to its ability to analyze and forecast the development and movement of key features, which are the tropical cyclones and typhoons.

Other than NOGAPS, some of the more skillful forecasting aides used by the JTWC are the One-way influence Tropical Cyclone Model (OTCM), the Colorado State University Model (CSUM), and the Climatological-Persistence Model (CLIP). OTCM is a regional primitive equation model developed by the U. S. Navy (Hodur and Burk, 1978), which takes its initial and boundary conditions from NOGAPS, smoothes the initial fields to get the steering currents, and then synthetically inserts the tropical vortex into the analysis much like NOGAPS does. On the other extreme, the CLIP model (Xu and Neumann, 1985) uses regression analysis to predict forecast tracks based on past motion of the present storm combined with historical data from storms in the same area. In the middle ground, the CSUM is a statistical-dynamical model (Newmann and Lawrence, 1975) that also uses regression equations to generate the track forecasts, but it includes information from dynamic model analyses and forecasts as predictors, as well as historical data.

Until recently, global models were not considered adequate to forecast tropical cyclone motion, since they could not resolve the small-scale atmospheric structures associated with these storms. Recent model improvements, however, have altered this commonly held opinion. For example, an independent study of NOGAPS forecasts for Northern Hemisphere Western Pacific storms during calendar year 1991 (Goerss, 1992) illustrated significant model skill. Figure 4 compares the performance of NOGAPS to the other forecasting aides described above, and to the official track forecast of JTWC. In each case, Goerss compared the forecasted position of the storm to the final "best track" data provided by JTWC. The median errors were computed for all storm tracks for each model for all forecast periods. The smallest track error in each case was provided by the global data assimilation system. Even more remarkable are the statistics shown in Table 1. In the early stages of tropical storm development, before any synthetic observations were assimilated into the analyses, NOGAPS was analyzing and forecasting the development of most of the named storms, with 79% of the storms detected in the 24-h forecast and 66% still maintained at 72 hours. Once the storms developed to the stage where synthetic observations were used to position the storms in the analyses, 87% of the storms in 1991 were still detectable in the 72-h forecast.

It is this skill that has lead us to revisit Keen's (1982) original hypothesis that westerly wind bursts were associated with tropical cyclone activity in the western Pacific, and that these wind events were somehow associated with the El Niño. If a relationship exists between westerly wind bursts and tropical cyclones, a model with the skill in the tropics exhibited by NOGAPS should be able to define this relationship better than individual observations can. Furthermore, by forcing an ocean circulation model with the surface wind stresses produced twice-daily by the NOGAPS model, we hope to determine the role of the westerly wind bursts in modifying the circulation in the eastern equatorial Pacific more precisely than can be determined by using monthly mean wind forcing (Kindle and Phoebus, 1994).
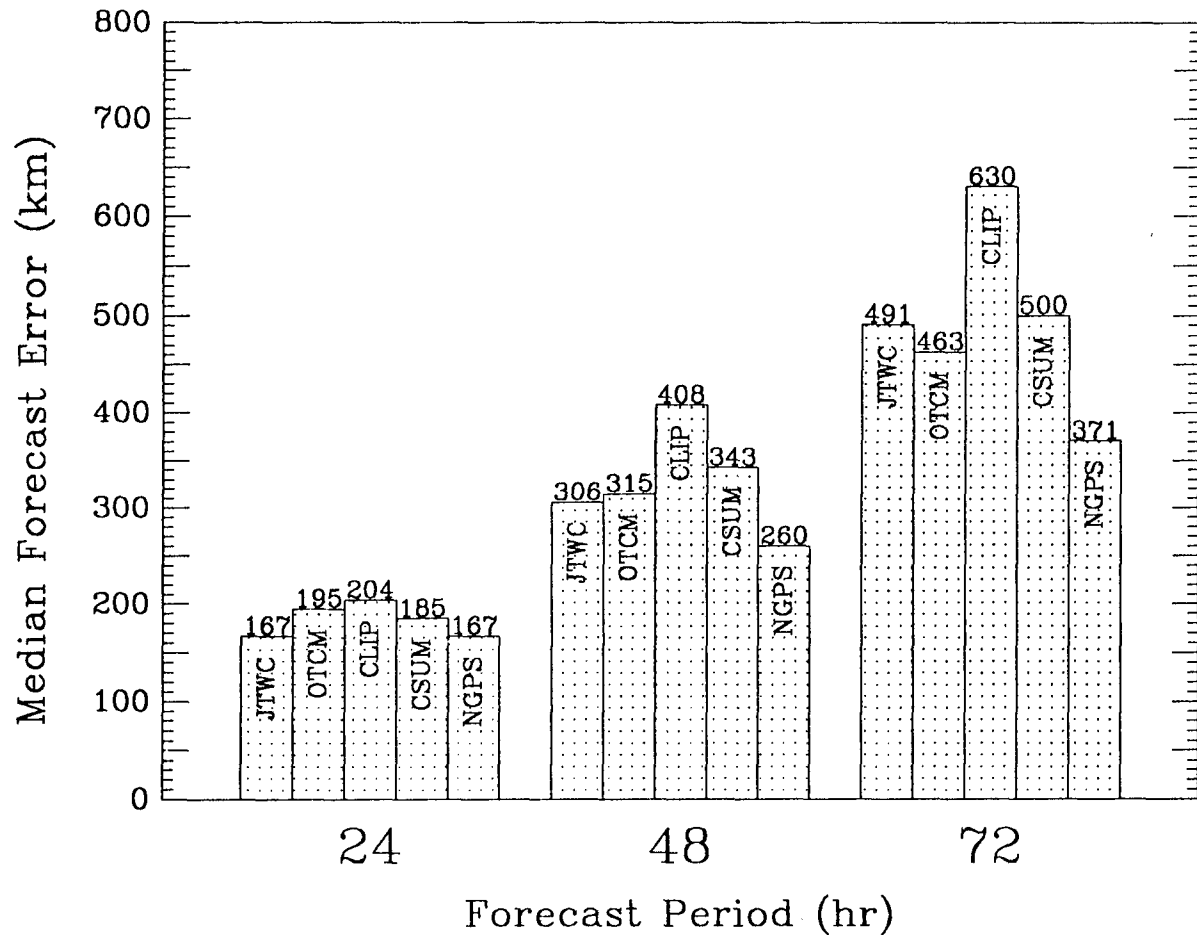
Fig. 4 – Median model forecast errors compared to the official JTWC forecast errors for the
1991 western Pacific tropical cyclone tracks

Table 1 – Impact of Synthetic Tropical Soundings on NOGAPS Tropical Cyclone Forecasting Skill

	Without synthetic obs			With synthetic obs		
Forecast period (hr)	24	48	72	24	48	72
Number of cases	56	112	168	300	246	192
Position error (km)	334	454	606	191	298	436
Storm detection (%)	79	77	66	96	90	87

4 MODEL DEPICTION OF WESTERLY WIND EVENTS

On occasion, the prevailing easterly trade winds in the tropics are replaced over small areas by episodes of very concentrated, highly energetic positive zonal winds (westerlies). These westerly wind bursts, while not unique to any one particular region, are most prevelant in the western equatorial Pacific. The anomalous westerlies may extend over more than 30 degrees of longitude and several degrees of latitude in the area between New Guinea and the dateline, and speeds of 10-15 m/s are not uncommon. Of particular interest are the events that occur within plus or minus 3 degrees of the equator, since this anomalous forcing can generate eastwardly propagating equatorially trapped Kelvin waves in the Pacific Ocean that may account for much of the quasi-periodic warming that occurs in the central and eastern Pacific (Giese and Harrison, 1990).

Traditional means of identifying westerly wind bursts rely upon wind measurements from ships, buoys, and islands. Isolated point measurements, however, cannot provide a complete picture of the nature of the westerly wind event. Other sources of information that have received less attention are the low-level wind fields that are produced by global atmospheric models, due in large part to their past poor performance in the tropics (Reynolds et al., 1989). However, many improvements have been made in recent years, and given the lack of observations in the area of interest, today's global data assimilation systems deserve another look. NOGAPS, with its sophisticated physics package and use of nonconventional data sources, is particularly well suited for tropical studies. While no model or analysis is perfect, we must recognize that observations are also contaminated by various sources of error, including instrument errors, recording or transmission errors, and errors of representativeness. Thus, we prefer to think of the model output as providing another estimate of the low-level wind field, and this depiction has the advantage of being fairly continuous in space and time and dynamically consistent.

To lend credibility to the analyzed and forecasted wind fields examined in this report, we will rely on information provided by JTWC, the Australian Bureau of Meteorology, and the Fiji Meteorological Service concerning the strengths and tracks of tropical cyclones in the western and central Pacific. Once a storm becomes strong enough that synthetic observations are automatically generated to initialize the storm in NOGAPS, the larger-scale circulation associated with the storm is clearly depicted and accurately positioned in the analysis. However, NOGAPS often analyzes these circulations days before the tropical depressions or tropical storms develop. Since such circulations are difficult to verify with observational data, if we can consistently track a circulation backward in time from a known tropical storm, we have some confidence that the circulation is real, even though its position may be somewhat misplaced.

Our efforts to detect westerly wind bursts using model output will concentrate on the period from October, 1990 through January, 1992. This period of time was chosen for several reasons. First, both the SSM/I data and synthetic tropical observations were being used operationally in the NOGAPS analysis. Second, the NOGAPS software components have remained relatively stable since that time. Last, there were indications that an El Niño was developing in late 1990 (Ropelewski and Smith, 1993), as SST in the central part of the Pacific basin increased, but the major warm event didn't appear further to the east until the winter of 1991-1992 (Fig. 5). Thus, looking at both winter seasons may provide added insight into the triggering mechanism(s) for the warm event.

The analyzed 10-m zonal wind component from NOGAPS, interpolated to six western Pacific locations, is plotted in Figure 6 for positive (westerly) values only. Comparison of the winds at different locations emphasizes how isolated observations can be misleading. A strong westerly wind at one location may not be supported by another point only a short distance away. For example, if the only platform reporting in December 1991 was at 156°E, 2°N, this major burst would not have been detected. Similarly, data from early May, 1991 illustrates that a significant westerly event can occur in the far western Pacific
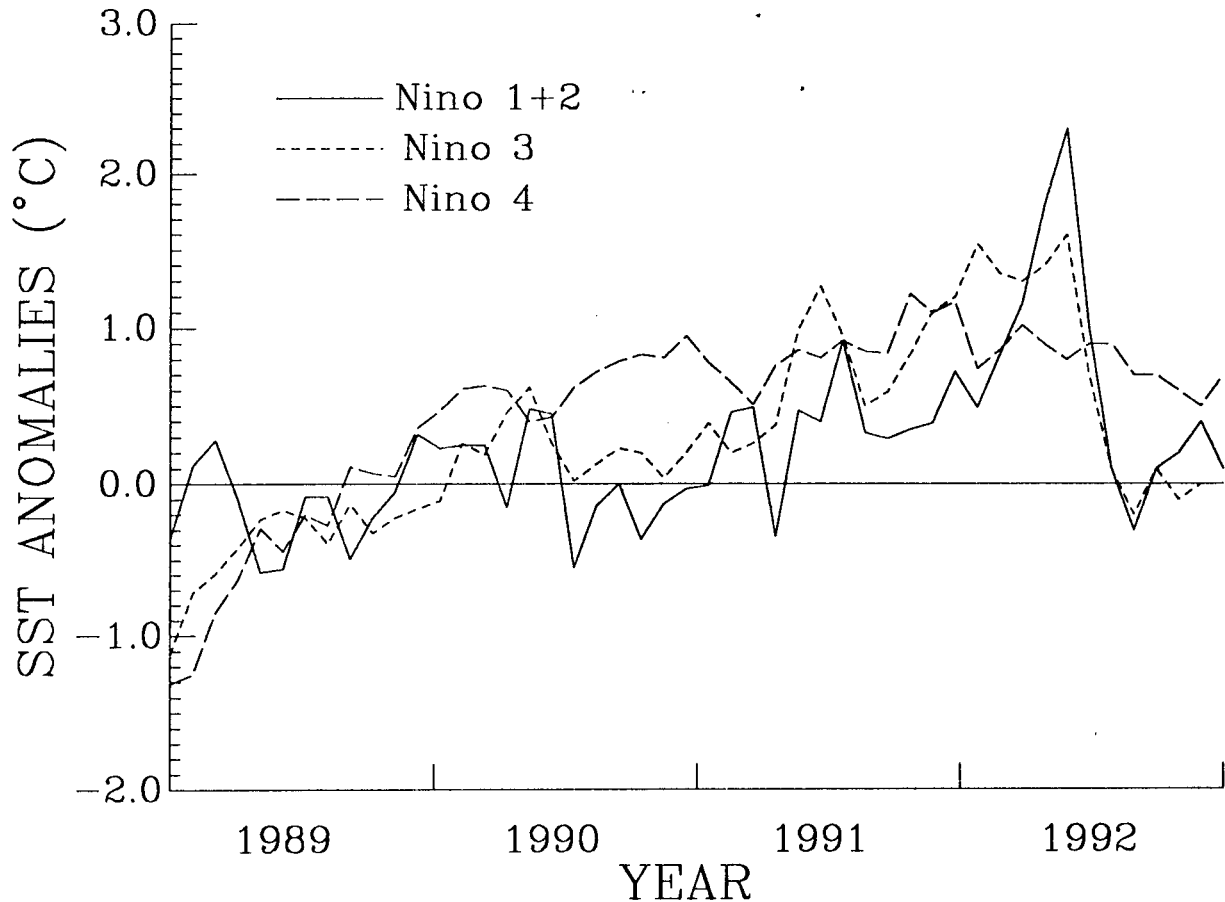
Fig. 5 – Sea-surface temperature anomalies (°C) in three El Niño areas, Nino 1+2 (0° to 10°S, 90°W to the
S. American coast), Nino 3 (5°S to 5°N, 150°W to 90°W), and Nino 4 (5°S to 5°N, 160°E to 150°W)

(see 156°E) but not be evident farther to the east (see 165°E). Since there are almost no islands near the
equator west of 165°E, such bursts would go undetected using conventional observations unless a ship or
buoy happened to be in the area. Of course, with the recent addition of more TAO buoys, this is less
likely now than in the past.

The corresponding TAO buoy data from five of the locations shown in Figure 6 were obtained from
NOAA's Pacific Marine Environmental Laboratory (PMEL). The zonal wind components measured by
the buoys are shown in Figure 7 for comparison. These records reflect all of the data available at PMEL,
not all of the observations available in real-time for the NOGAPS analysis. Receipt of the TAO buoy data
at FNMOC (via GTS) during the period of this study was somewhat limited. On most occasions, little if
any of the TAO buoy observations were available, so comparisons of the model to these buoy data provide
a quasi-independent means of verifying the NOGAPS analyses. For example, no TAO buoy data were
available at all from mid-October, 1991 through early January, 1992 due to satellite transmission and
processing problems, yet there is still close agreement between the analysis and the buoy observations.
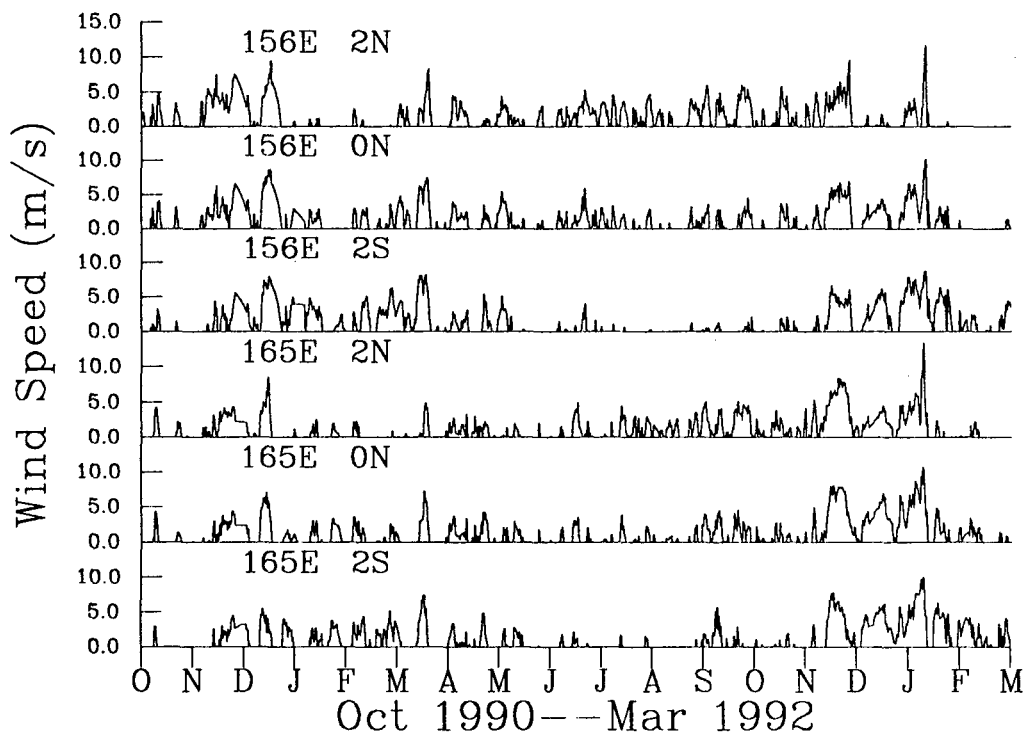
Fig. 6 – The NOGAPS 10-m zonal wind component (m/s) interpolated to six TAO buoy locations. Only positive (westerly) values are shown.
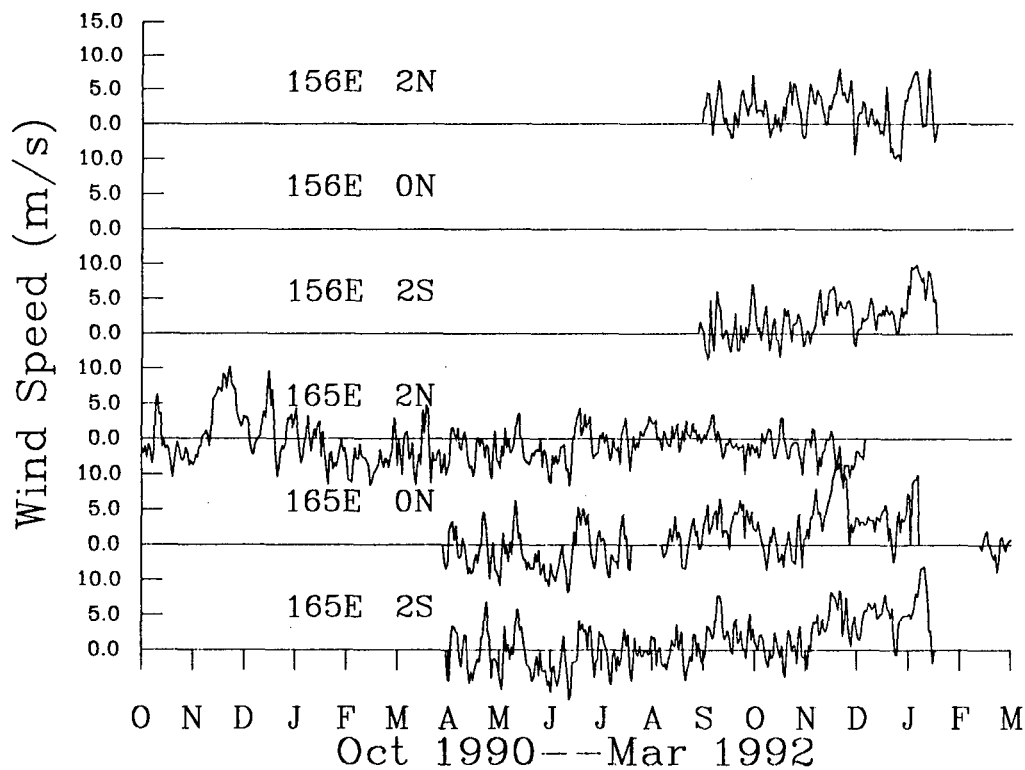

Fig. 7 – The observed zonal wind component (m/s) at fiveTAO buoy sites. Continuous records were not available at each site.

One glaring exception occurs at the 165°E, 2°N buoy location, where from September, 1991 on, few westerlies were measured, while strong westerly winds were recorded by the other buoys and depicted by the model. While this situation may seem comparable to the December, 1991 case, where the westerly burst was evident everywhere except at 156°E, 2°N, there are notable differences. It will become clear from later figures that the December, 1991 burst was associated with a pair of Southern Hemisphere cyclones that developed far to the east, leaving the most northwestern point of our array outside the westerly flow. However, in the other case, a supertyphoon formed at 4°N, 166°E in late November. It is hard to imagine how a point 2 degrees directly south of a developing typhoon did not experience westerly winds. Thus, we conclude that the observations from this buoy during the latter part of 1991 are probably in error. Had this data been available to the analysis, the NOGAPS quality control programs would most likely have rejected these observations, given that the surrounding data disagree significantly. The buoy in question apparently dropped off-line in December, 1991.

For a closer buoy/model comparison, the zonal wind component observed by the moored buoy at 2°N, 165°E is plotted along with the NOGAPS analyzed 10-m zonal wind component through the first half of the study (Fig. 8a), while the 0°N, 165°E location is shown for the remainer of the period (Fig. 8b). For the most part, the NOGAPS analyzed winds agree closely with the winds measured by the buoys. Although NOGAPS sometimes underestimates the strength of the wind, the stronger westerly events can be easily identified from either dataset. Since we are primarily concerned with strong zonal westerly forcing on the ocean, the weaker westerly wind components are not of interest here.

The major westerly wind events are readily apparent within these time series, and we will look at several of the more significant cases in detail. Since we are particularly interested in the relationship between westerly wind events and tropical cyclone development, we have made extensive use of information from the Annual Tropical Cyclone Reports published by JTWC (1991; 1992; 1993). The JTWC storm strengths and positions for the Northern Hemisphere systems are supplemented by storm track information provided by the Australian Bureau of Meteorology and the Fiji Meteorological Service (1992) for the South Pacific storms. To make the discussion easier to follow, some basic tropical storm terminology is given in Table 2 for the various stages of tropical cyclone development (although wind speed criteria are normally defined in knots). While convention is that tropical systems are not officially named until they reach tropical storm strength, to simplify our discussion of the various events, we have taken some leeway with convention, and will use the official names to distinguish the different storms at all stages of their development. Furthermore, we will use tropical cyclone (lower case) in the generic sense to refer to any tropical circulation, regardless of strength.

Table 2 – Western Pacific Tropical Cyclone Terminology

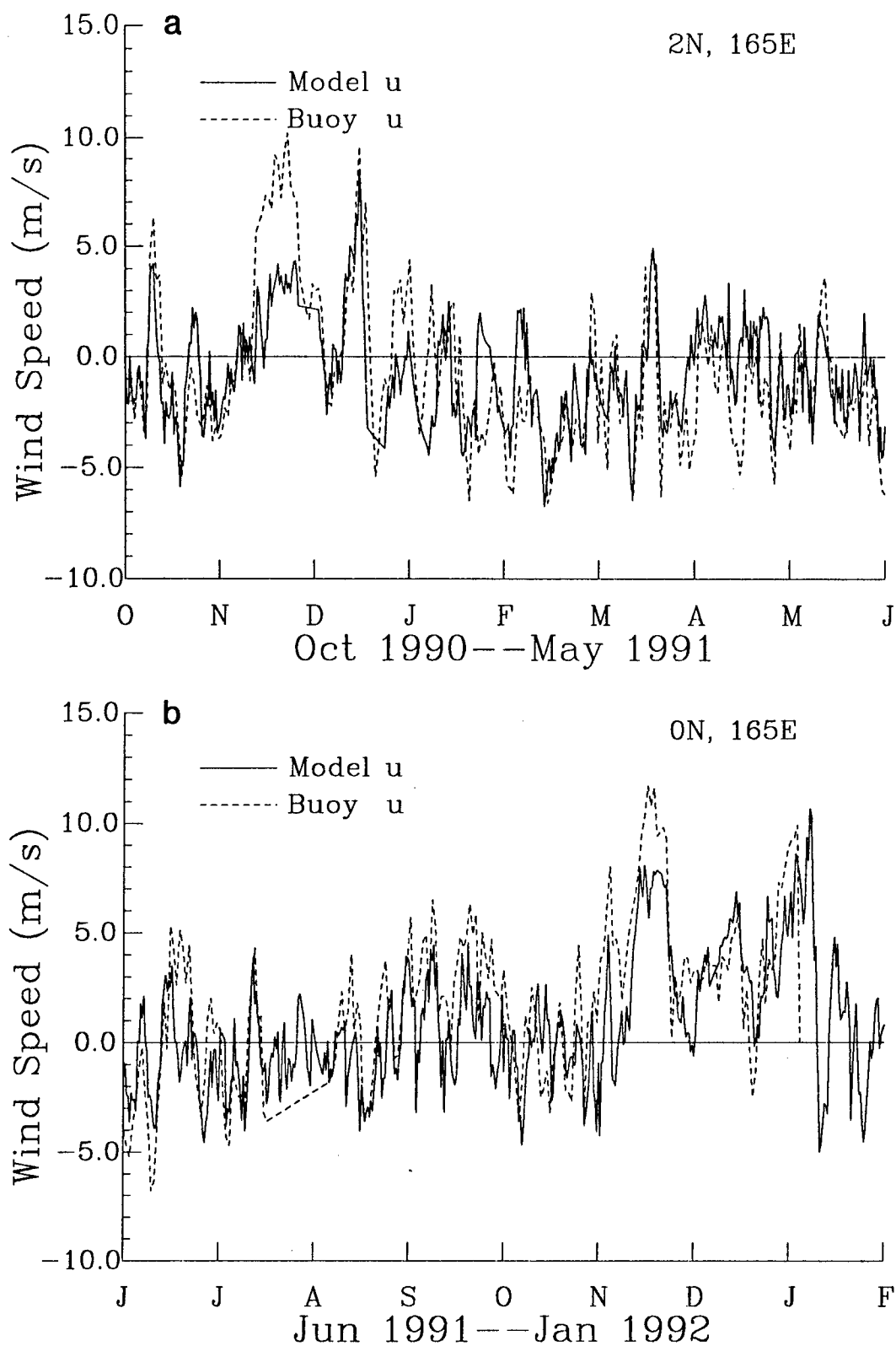| Maximum Sustained Wind Speed (ms^{-1})	Northern Hemisphere	Symbol	Southern Hemisphere
$\geq$ = 10.3	Tropical Disturbance	O	Tropical Disturbance
$\geq$ = 12.9	Tropical Depression	●	Tropical Depression
$\geq$ = 18.0	Tropical Storm	ᶘ	Tropical Storm
$\geq$ = 33.5	Typhoon	ᶘ	Tropical Cyclone
$\geq$ = 69.5	Supertyphoon	ᶘ	Severe Tropical Cyclone

Fig. 8 – A comparison of the NOGAPS 10 m zonal wind component (m/s) to the observed zonal wind component at a) 2°N, 165°E, and b)°0, 165°E

Prior to their appearance as organized tropical disturbances, some of the tropical cyclones can be traced backward in time to waves in the easterlies, which are migratory disturbances that move from east to west, imbedded in the easterly flow (Riehl, 1954). These easterly waves are often associated with weak troughs of low pressure and may be accompanied by active convection. In a streamline analysis, they will appear as slight waves in the otherwise zonal flow. As an easterly wave passes an observing platform in the Northern Hemisphere, easterlies would turn to northeasterlies, then to southeasterlies before becoming easterly once again behind the wave. As the easterly wave begins to intensify, the circulation becomes more cyclonic and the first true westerlies appear along the southern flank of the Northern Hemisphere circulation.

The following series of figures is presented to provide a more complete spatial and temporal picture of the relationship between the westerly wind bursts and the development of tropical cyclones. In each case, a series of snapshots of the low-level wind fields from NOGAPS are annotated with the symbols from Table 2 that depict the various stages of tropical cyclone development. The wind flow patterns are represented by streamlines, while the areas where the zonal westerly wind component exceeds 2.5 m/s are contoured and shaded every 2.5 m/s. While a global model cannot accurately analyze the true scale and maximum intensity of a tropical cyclone, it can capture the larger-scale flow that surrounds the tropical cyclone and will produce much stronger winds and tighter circulations as the storms develop. The next few sections are organized by season, since from Figure 6 it is clear that each hemisphere experiences more episodes of westerlies during their respective summer seasons, while the stronger bursts occur during the Northern Hemisphere fall and winter seasons.

4.1 Fall 1990

The month of November, 1990 is dominated by the development of three Supertyphoons in the western North Pacific and a strong Tropical Cyclone in the South Pacific (Fig. 9). Distinct pockets of westerlies are found along the inflow regions of each cyclone, although at times these pockets of westerlies are connected by weaker westerly winds. For the most part, the westerlies are confined to the area between the equator and 10N, and at times there are strong westerlies present in the equatorial waveguide.

The development of Mike and Page is shown in Fig. 9a-c. NOGAPS has trouble positioning the cyclones initially, but by November 9 clearly shows two distinct cyclones, with the strongest westerlies south of the stronger storm and extending westward to where Tropical Storm Nell is located in the South China Sea. These westerlies increase as Mike reaches supertyphoon strength on November 11. The model position of Page remains too far south and west but improves as Page becomes a tropical depression on the 16th. In Figure 9d-f, Page is now the westernmost cyclone and NOGAPS is analyzing another cyclone to the east (Owen). JTWC has been tracking this disturbance since November 15, when it was located east of the dateline. While NOGAPS did not pick up the disturbance that soon, from this point on the model does an admirable job of depicting the storms, even before synthetic observations are inserted. There is also some hint of a new circulation in the Southern Hemisphere east of the dateline on November 19. Each of the circulations is associated with a distinct westerly wind patch.

The first of these three cyclones to reach tropical storm strength is Owen, which is upgraded at 12Z on November 21, followed closely by Page at 00Z on November 22 and later by Sina at 00Z on November 25. The equatorial westerlies are most extensive on November 24 (Fig. 9e), although the strongest wind speeds are well north of the equator. The flow around Owen and Sina forms a continuous band of westerlies along the equator from 145°E to 175°E, still separated somewhat from the westerlies south of Page. The magnitude of the zonal wind component in the equatorial waveguide is primarily in the range of 2.5-7.5 m/s, with small areas exceeding 7.5 m/s. Three days later (Fig. 9f), the three storms
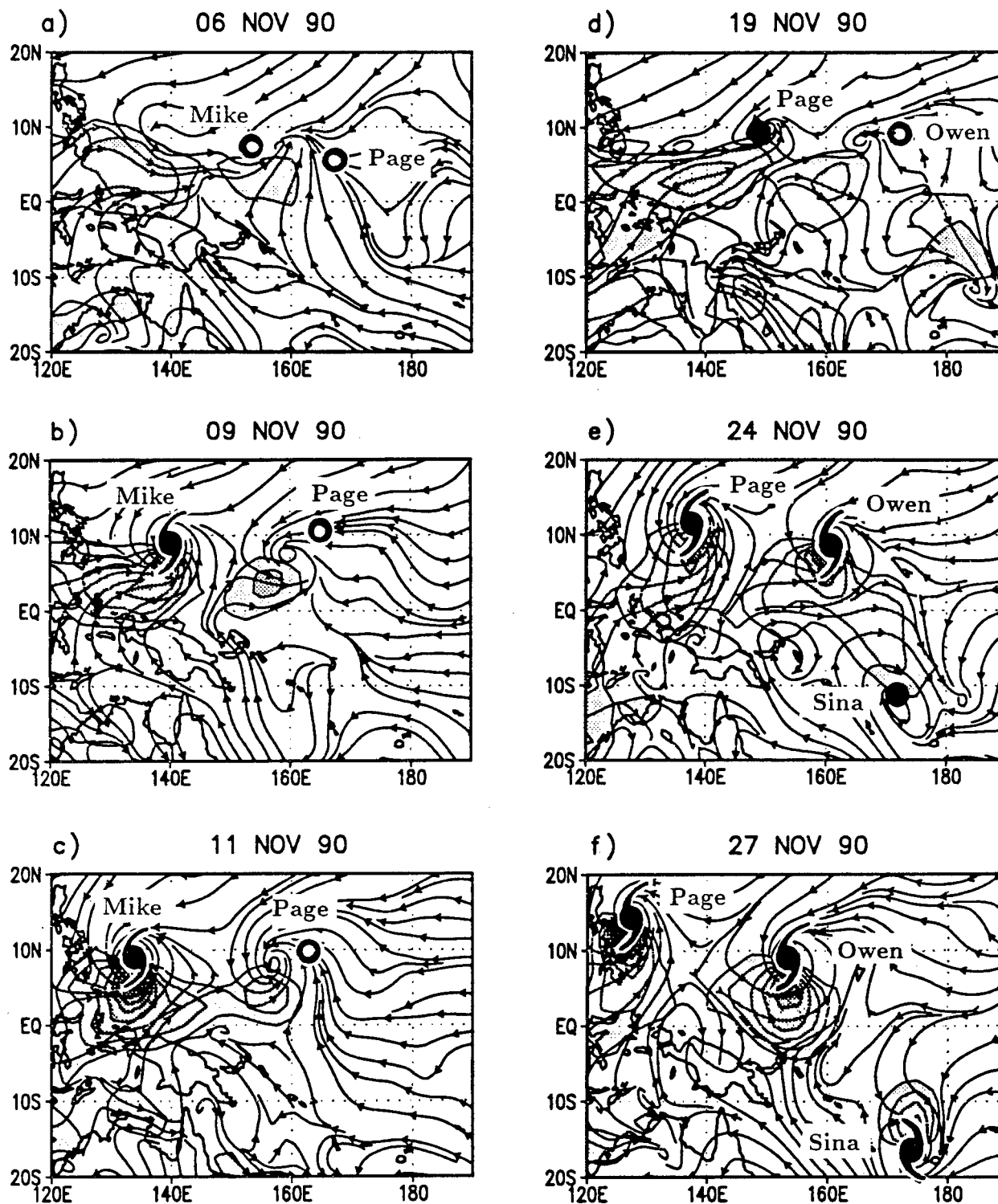
Fig. 9 – NOGAPS 1000-mb streamline analyses (00Z), with westerly u-components greater than 2.5 m/s contoured and shaded every 2.5 m/s. Official cyclone positions are noted by the appropriate symbol. a) November 6,1990, b) November 9, 1990, c) November 11, 1990, d) November 19, 1990, e) November 24, 1990, f) November 27, 1990

are at their maximum intensities, with both Supertyphoons Page and Owen having winds over 70 m/s and Sina with sustained winds of 62 m/s. As the storms separate and move away from the equator, the extremely zonal fetch of westerlies along the equator begins to break down, and the westerlies retreat along with the storms. Owen, which is still south of 10°N, continues to impact the equatorial waveguide, but the influence of the other two storms is negligible.

By early December, the flow becomes more cross-equatorial and there are almost no westerly winds evident in the western equatorial Pacific. What follows is the classical development of a pair of tropical cyclone twins, which typically occur in this region only about once every two or three years (Lander, 1990). The first hint of a coupled cyclonic circulation appears in the NOGAPS wind field on December 9 (Fig. 10a), and weak westerly winds appear between the two vortices. For several days, the westerly winds remain confined to this narrow band. Then, on December 13, JTWC notes a tropical disturbance in the Northern Hemisphere, within the larger scale circulation analyzed by NOGAPS (Fig. 10b). At the same time, the westerlies have strengthened and extended westward from their initial position around the dateline, more or less centered on the equator and terminating near the longitude of the coupled cyclones. Zonal wind speeds now exceed 7.5 m/s in a small area near the center of the westerly wind patch.

As the northern cyclone continues to develop, the band of westerlies intensifies and the fetch increases to the west (Fig. 10c). While a broad area along the equator is experiencing wind speeds of 5-10 m/s, the strongest winds are still located north of the equator, closer to the southern edge of Tropical Storm Russ. As the coupled circulations progress westward, the southern cyclone (Joy) begins to strengthen (Fig. 10d). Note that as the the storms strengthen, they not only move west, but they begin to separate and move away from the equator (Fig. 10e,f). Although the westerlies continue to increase in speed, the centers of maximum wind speed move away from the equator with the separating storms. Thus, the westerly forcing in the equatorial waveguide is often reduced during the stronger stages of the tropical cyclones. Where the westerlies reached as far east as 175°E on December 13, by December 22 they only extend to 150°E.

While this pattern repeats what was observed in the model during the November event, it differs in that the December burst is more symmetric about the equator, due to the almost simultaneous development of the Russ/Joy couplet along the same longitude, both very near the equator. Although the November burst was also accompanied by both Northern and Southern Hemisphere storms, their circulations did not appear to be as directly coupled, as Sina developed further south of the equator than Joy and also further east of its northern hemisphere counterpart, Owen. The series of tropical storms described above were associated with westerly wind anomalies that persisted in the western equatorial Pacific for the better part of November and December of 1990. Taken together, the forcing from these westerly bursts generated a significant response in the ocean, resulting in a 25-cm rise in SSH in the eastern equatorial Pacific between mid-December, 1990 and the end of January, 1991 (Kindle and Phoebus, 1994). However, the anticipated El Niño failed to appear.

4.2 Winter 1991

Some westerlies persisted into January and February of 1991, mainly south of the equator with the onset of the Australian monsoon. Throughout this period, which is the active tropical cyclone season in the southern hemisphere, a number of low-level cyclonic wind circulations are analyzed by NOGAPS. Tw tropical storms develop in the Southern Hemisphere in mid-February, one just east and one just west of Australia, both between 15-20°S. Strong westerly winds are present from the Indian Ocean across northern Australia and into the western Pacific around 10°S, but there is no strong westerly forcing on the ocean along the equator.
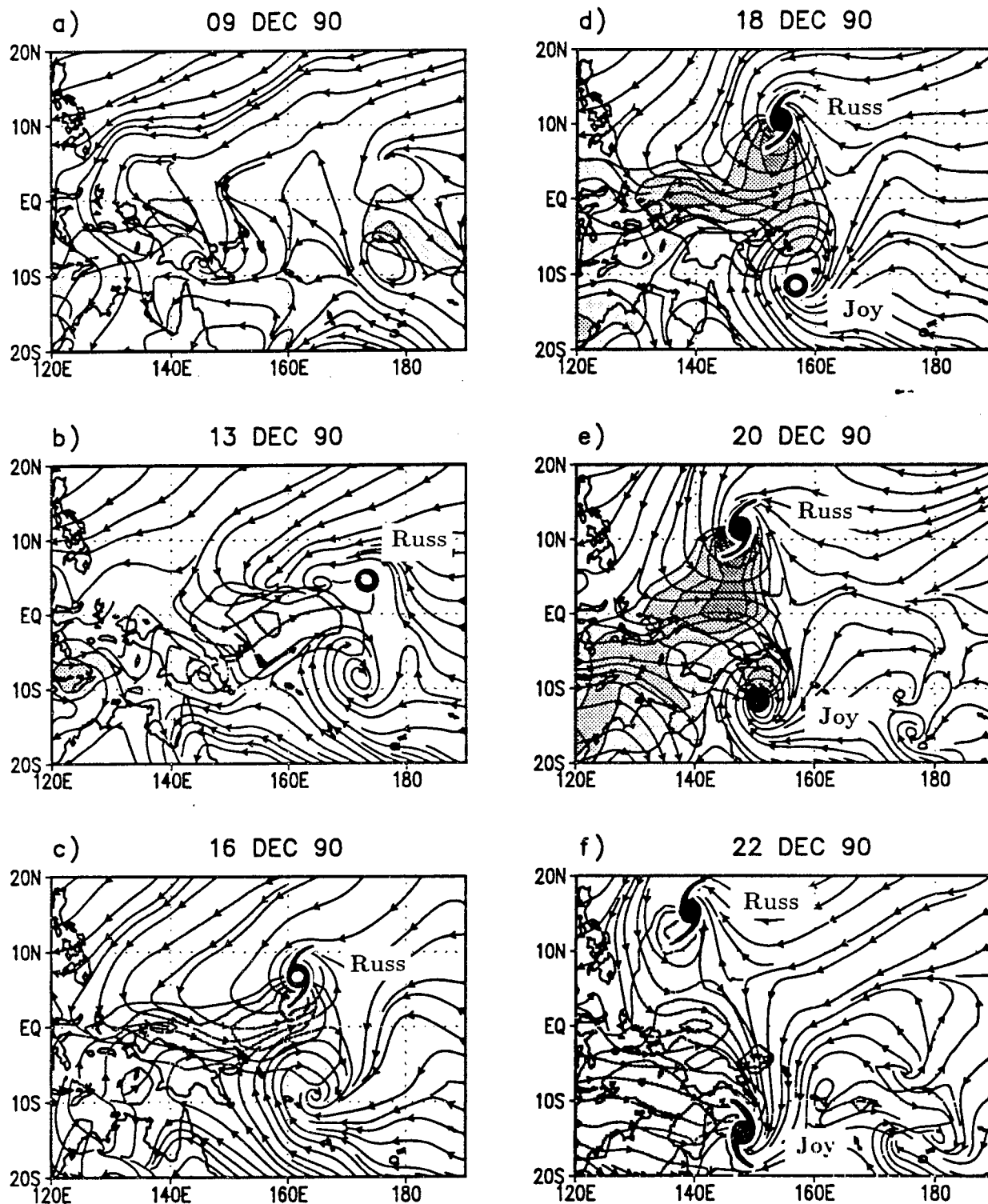
Fig. 10 – Same as Fig. 9, but for a) December 9, 1990, b) December 13, 1990, c) December 16, 1990,
d) December 18, 1990, e) December 20, 1990, f) December 22, 1990

From Figure 8, the next notable westerly wind burst in the equatorial waveguide occurs from late February through late March, 1991. The Australian monsoon is well established, with strong westerly winds dominating the flow between the equator and 15°S. On February 23, Tropical Storm Kelvin develops over the Gulf of Carpentaria and moves across the Cape York Peninsula of Australia out into the South Pacific Ocean, while another circulation is analyzed near the eastern terminus of the westerlies around 175°E (Fig. 11a). The eastern cyclone moves closer to Kelvin and shortly thereafter, NOGAPS begins to show a new circulation just north of the equator around 155°E (Fig. 11b). The strongest westerlies are now present in the inflow regions of these cyclones. Over the next few days, this flow pattern changes very little, but the other two cyclones begin to intensify while Kelvin drifts slowly north (Fig. 11c).

The development of the northern cyclone (Sharon) appears to have the most impact on the equatorial waveguide, as the stronger winds shift northward and become more centered along the equator. The peak of the equatorial westerlies occurs from March 3-7 (Fig. 11c-e), when Sharon progresses from a tropical disturbance to a tropical depression. As the two Southern Hemisphere cyclones dissipate, Sharon reaches tropical storm strength and moves more rapidly to the northwest (Fig. 11f), reducing the fetch of the westerlies. Although the wind speeds continue to strengthen, the wind maximum moves further north of the equator.

The absence of westerly winds along the equator east of 150°E is short-lived, for as Sharon approaches the Phillipines, NOGAPS analyzes a new northern/Southern Hemisphere cyclone couplet between 150-160°E, with the northern vortex almost right on the equator (Fig. 12a). The westerly winds between these circulations increase in fetch and intensity as the Southern Hemisphere cyclone develops into a tropical depression (Fig. 12b,c). Between March 14 and 15, the westerly band becomes very zonal and wind speeds increase over a broad area, exceeding 7.5 m/s over almost 20° of fetch. Little change is observed in the analyses until March 18, when the Northern and Southern Hemisphere circulations become more longitudinally aligned. The westerlies now extend over 40° of longitude, from 130-170°E, between and to the west the two cyclones, with wind maximums located in the inflow regions of each cyclone (Fig. 12d). As the northern hemisphere cyclone develops, the southern cyclone moves rapidly south (Fig. 12e) and no longer influences winds in the equatorial waveguide. The northern storm becomes Tropical Cyclone Tim at 18Z, March 21. As Tim continues to strengthen, it moves north and west (Fig. 12f), soon leaving only remnants of the previous equatorial westerlies.

Figure 13a compares the total wind speed at 150°E, 0°N to the magnitude of the zonal wind component from late February through late March. While the u -component is positive (westerly) during this entire time, there are two distinguishable periods when the wind becomes very zonal, in other words, the meridional component of the wind is almost zero. The first westerly burst begins on March 2, peaks on March 5, and ends on March 9. The second burst begins on March 13, increases dramatically between the 14th and 15th, and continues through the rest of the time shown.

Annotated on the same figure are the time lines showing the stages of development for the tropical cyclones associated with the winds at that point. For example, Sharon becomes a tropical disturbance just after the increase in westerly wind speed on March 3 and strengthens to a tropical depression on the 5th following the second increase in the westerlies. By the time Sharon becomes a named tropical storm on the 7th, it is located closer to 145°E, west of the point shown here, and the wind speeds at 150°E begin to drop. Later in the month, the increase in wind speed from March 14 to 15 is associated with the transition of 16P from a tropical disturbance to a tropical depression. The influence of Tim is better seen at 160°E (Fig. 13b). As with Sharon, by the time Tim becomes a tropical storm on the 21st, it is located 5 degrees west of 160°E, so wind speeds at 160°E are decreasing while we see an increase at 150°E (Fig. 13a).

a) 24 FEB 91

b) 27 FEB 91

c) 03 MAR 91

d) 05 MAR 91

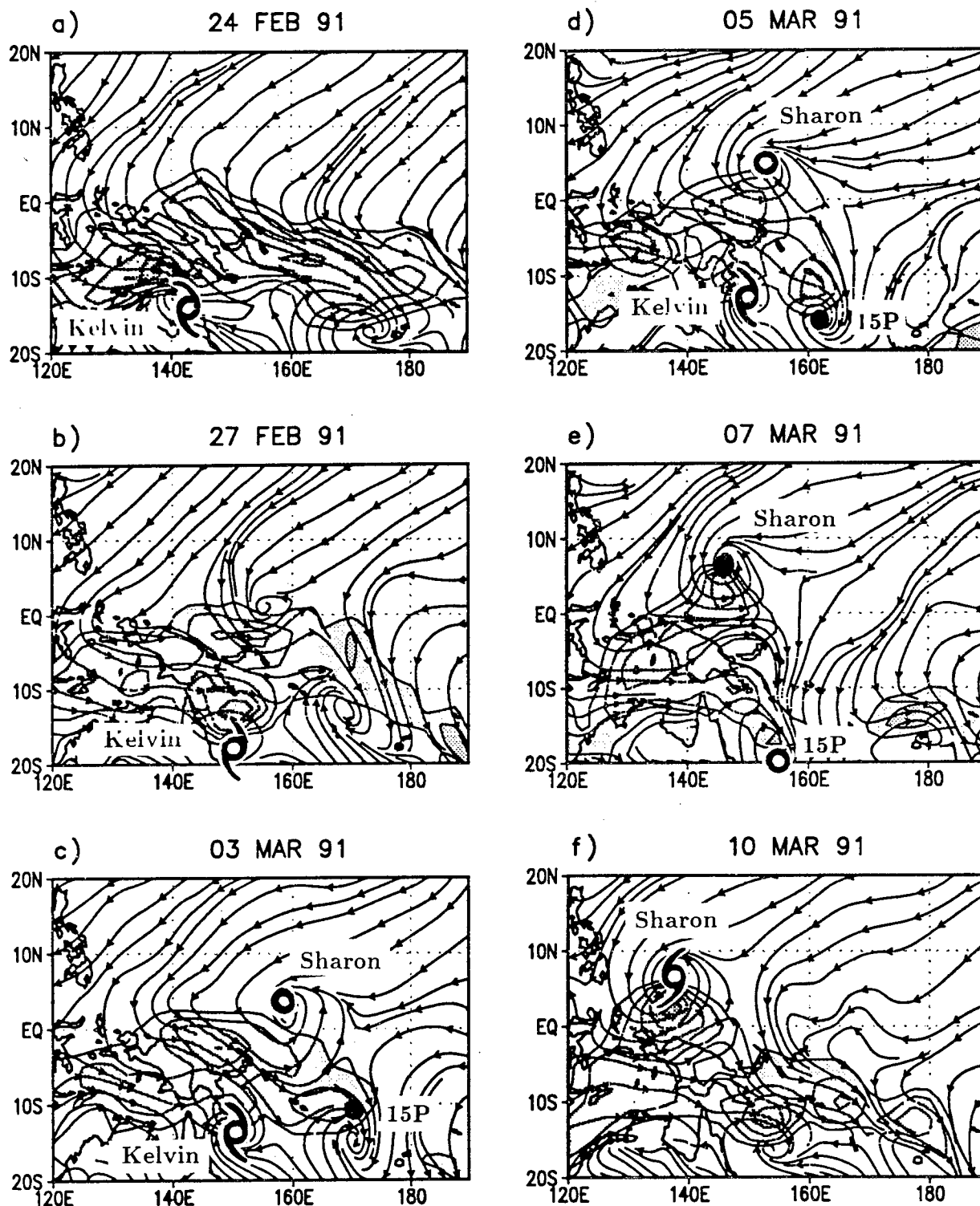**e)** 07 MAR 91

f) 10 MAR 91

Fig. 11 – Same as Fig. 9, but for a) February 24, 1991, b) February 27, 1991,
c) March 3, 1991, d) March 5, 1991, e) March 7, 1991, f) March 10, 1991

a)   13 MAR 91

d)   18 MAR 91

b)   14 MAR 91

e)   20 MAR 91
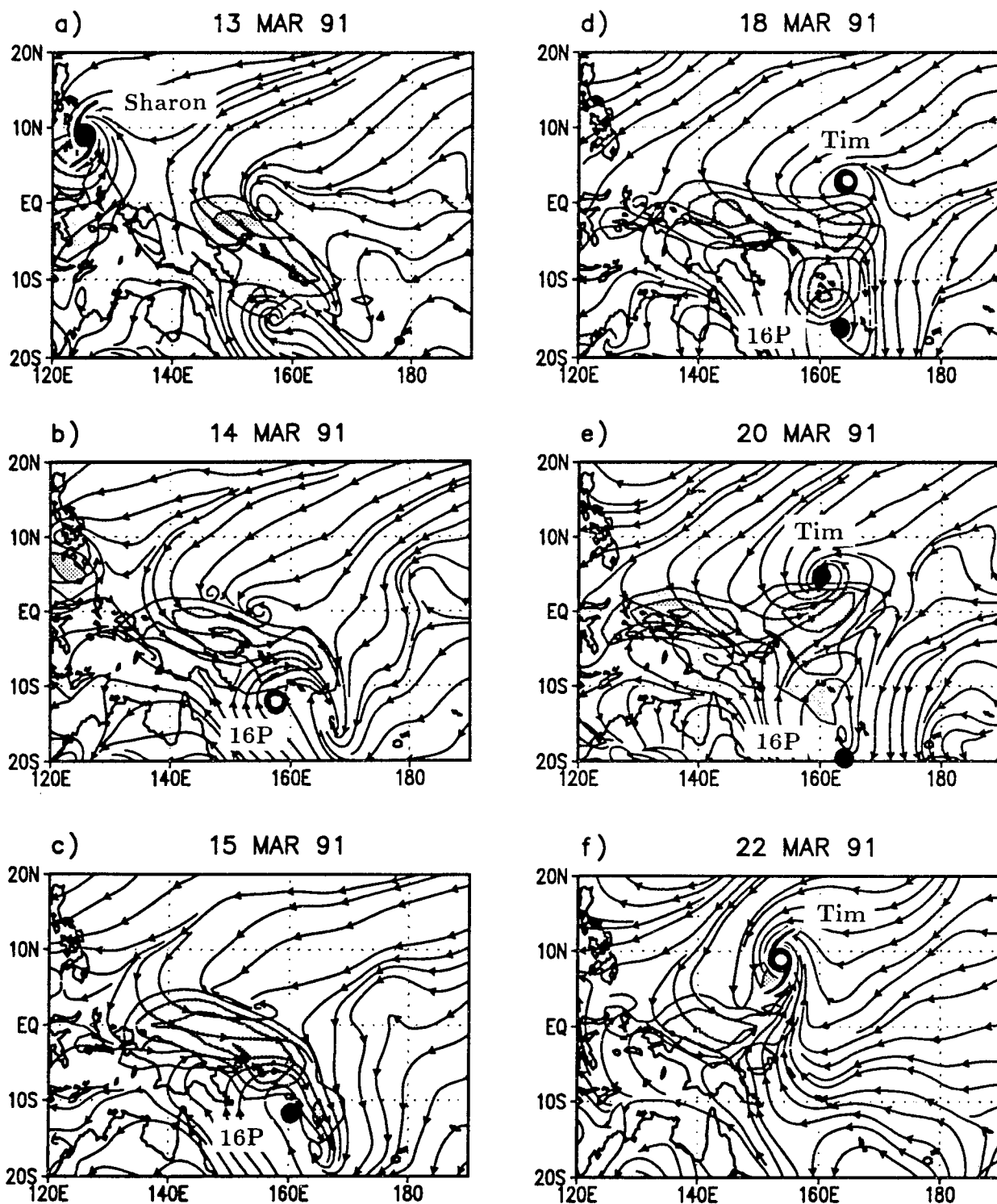
c)   15 MAR 91

f)   22 MAR 91

Fig. 12 – Same as Fig. 9, but for a) March 13, 1991, b) March 14, 1991,
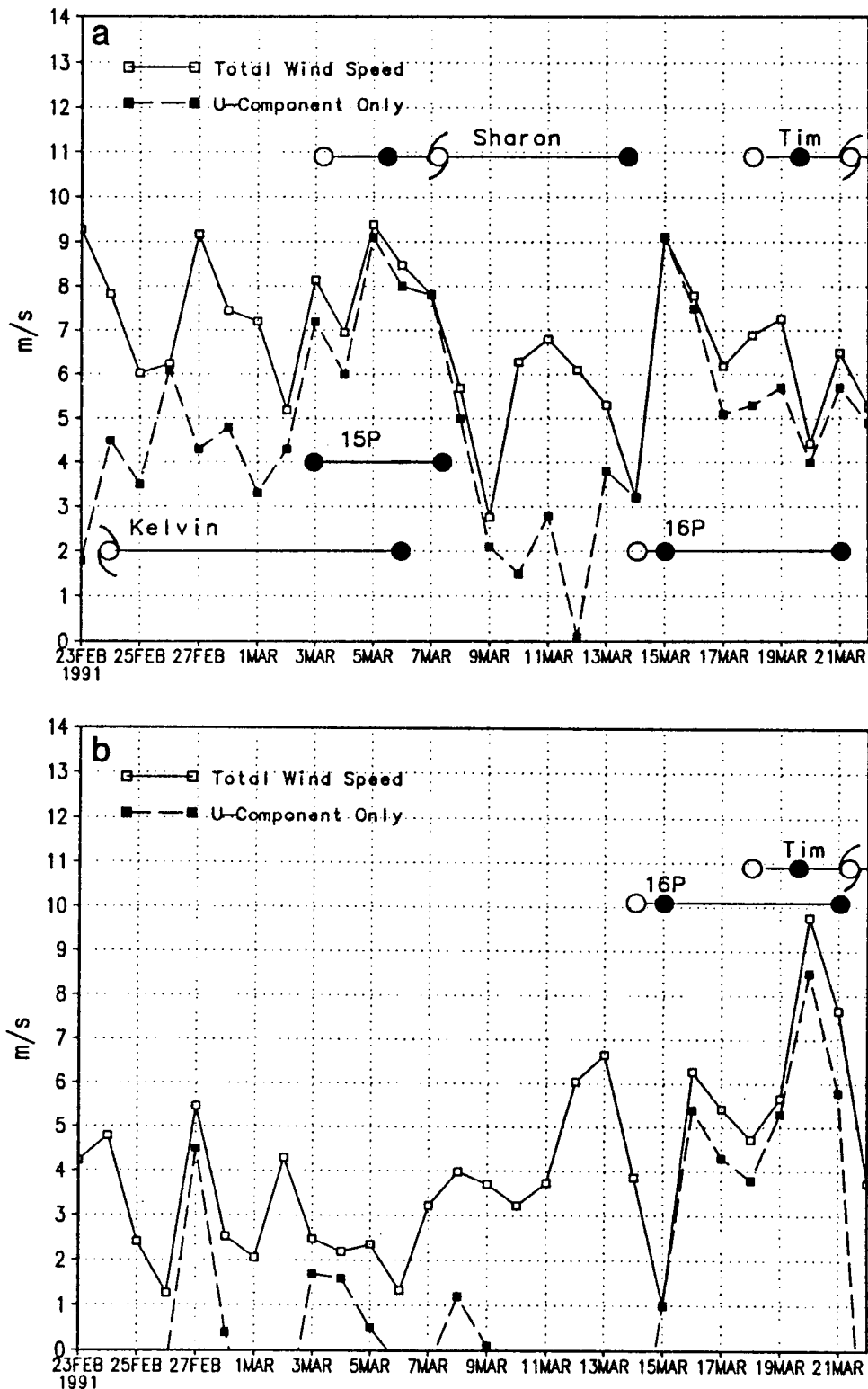c) March 15, 1991, d) March 18, 1991, e) March 20, 1991, f) March 22, 1991

Fig. 13 – Single-point time series of NOGAPS 1000-mb wind speed compared to the zonal wind component only at (a) 150°E, 0°N and (b) 160°E, 0°N. Time lines of cyclone development are annotated.

In both of the March, 1991 cases, the westward movement of the storms is further reflected in the time-longitude series shown in Figure 14. It has been suggested that westerly winds in the western Pacific are related to surges of westerlies from the Indian Ocean in association with the 30-60 day oscillations (Lau et al., 1989). While Figure 13 gives some indication that the westerlies increase just prior to the next stage of cyclone development, Figure 14 does not indicate that there is much of a signal propagating from the Indian Ocean. The predominant signal in this time-longitude series of equatorial winds is the westward propagation of the westerlies, at least during this limited time period. The westerlies appear to develop on location in late February and then propagate slowly westward during the first half of March, reflecting the westward movement of Sharon. During the latter half of the month, another distinct area of westerlies develops around the same location as the first series. In this case, there is perhaps a slight eastward propagation of the wind maximum, but by the end of the time series, the eastward extent of the westerlies is decreasing as Tim moves westward.

4.3 Spring-Early Fall 1991

By the end of March, the western equatorial Pacific is once again in an easterly wind regime (Fig. 8). Early in April, small areas of westerly winds are analyzed along the equator, once again associated with cyclonic circulations developing on easterly waves. While some convection can be seen in these areas from satellite imagery, none of these circulations develops into anything significant. However, the near-equatorial trough is re-established, and later in April, tropical storm Vanessa forms around 5°N, 140°E. The equatorial westerlies associated with Vanessa are confined to the far western Pacific and by April 27, Vanessa has moved into the South China Sea and most of the westerly winds along the equator have disappeared.

Early May brings the development of another set of dual-hemisphere cyclone twins, which form around 150°E as illustrated in the series of analyses shown in Figure 15. The northern cyclone becomes Supertyphoon Walt and the southern cyclone becomes Tropical Cyclone Lisa. The pattern of development is somewhat different from that seen previously. In this case, the first westerlies are evident along the equator between two cyclonic circulations around 140°E, and an easterly wave is present around 165°E (Fig. 15a). As the easterly wave moves into the eastern edge of the westerlies, two new cyclonic circulations develop around 155°E (Fig. 15c). This pattern agrees with the findings of Heta (1990), who showed that tropical cyclones in the western Pacific originate as easterly waves within the trade winds, with development most often occurring when the waves enter the area of convergence generated by the westerly anomalies. Heta noted that there was frequently a surge in the westerlies just prior to the development of the tropical disturbance. There is some evidence of that scenario in this case, as well.

This is one of the only westerly bursts that we have seen where the westerlies were present before the initial signs of the developing tropical storms, although even in this case, weak cyclonic circulations around 140°E accompany the first westerlies. Satellite imagery from May 3 shows convection along the equator from 120-150°E, where the initial westerlies are present, with two additional convective masses around 150-160°E, between 5-10°N and 5-10°S. These areas correlate well with the flow patterns seen in NOGAPS and with the description of cyclone twin development given by Lander (1990). As the two cyclones around 155°E begin to dominate, the pattern of development is similar to that observed with the Russ/Joy couplet. The maximum westerly winds are concentrated between the two disturbances, and as the storms develop and track away from the equator, two distinct areas of westerly winds move with them (Fig. 15d-f).

As seen in Figure 6, the Northern Hemisphere summer season exhibits some westerly wind periods, but the locations of the stronger westerlies are mostly north of the equator. The only exception is in the latter part of June, when a monsoon depression forms very near the equator. A strong short-lived burst
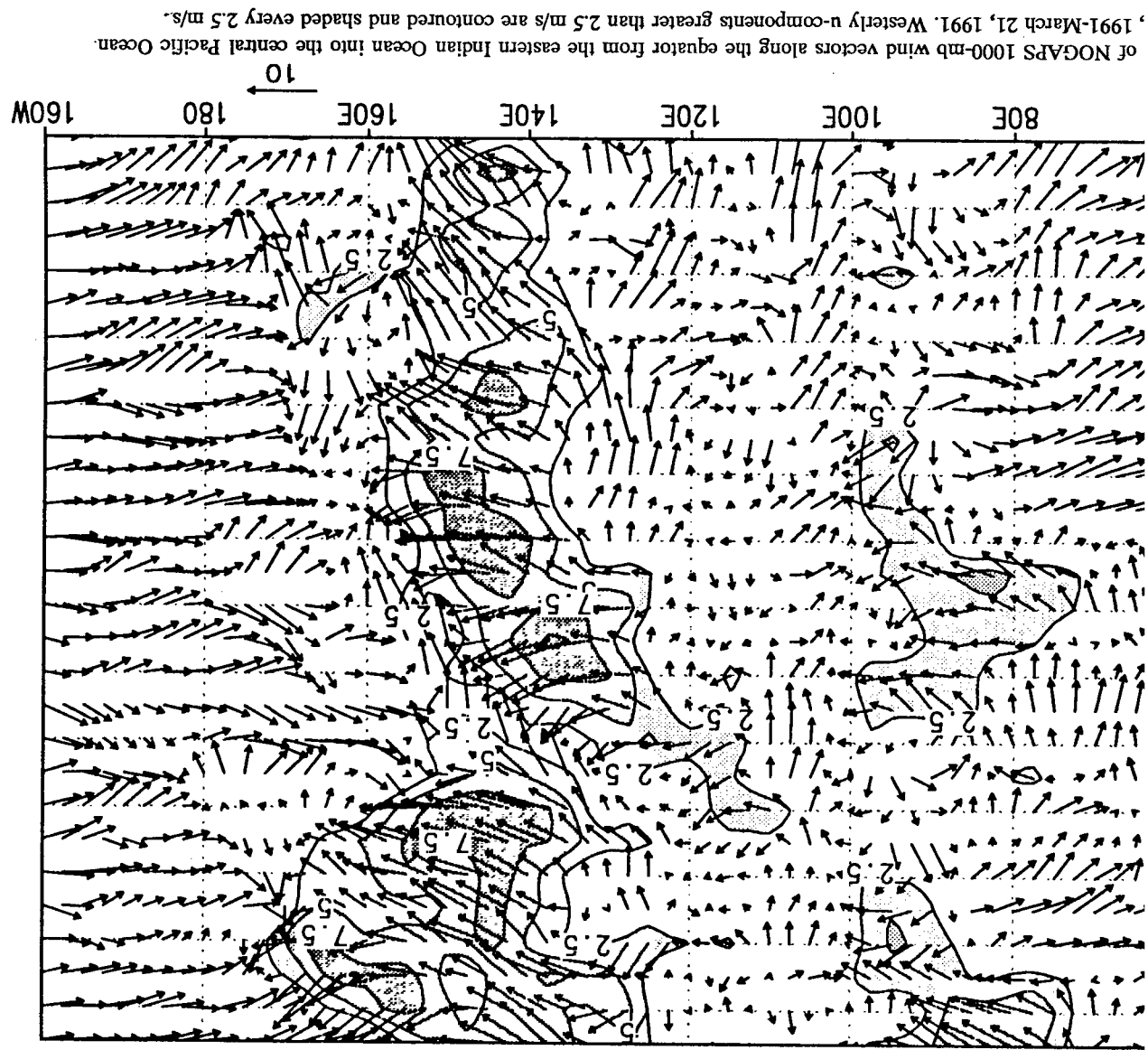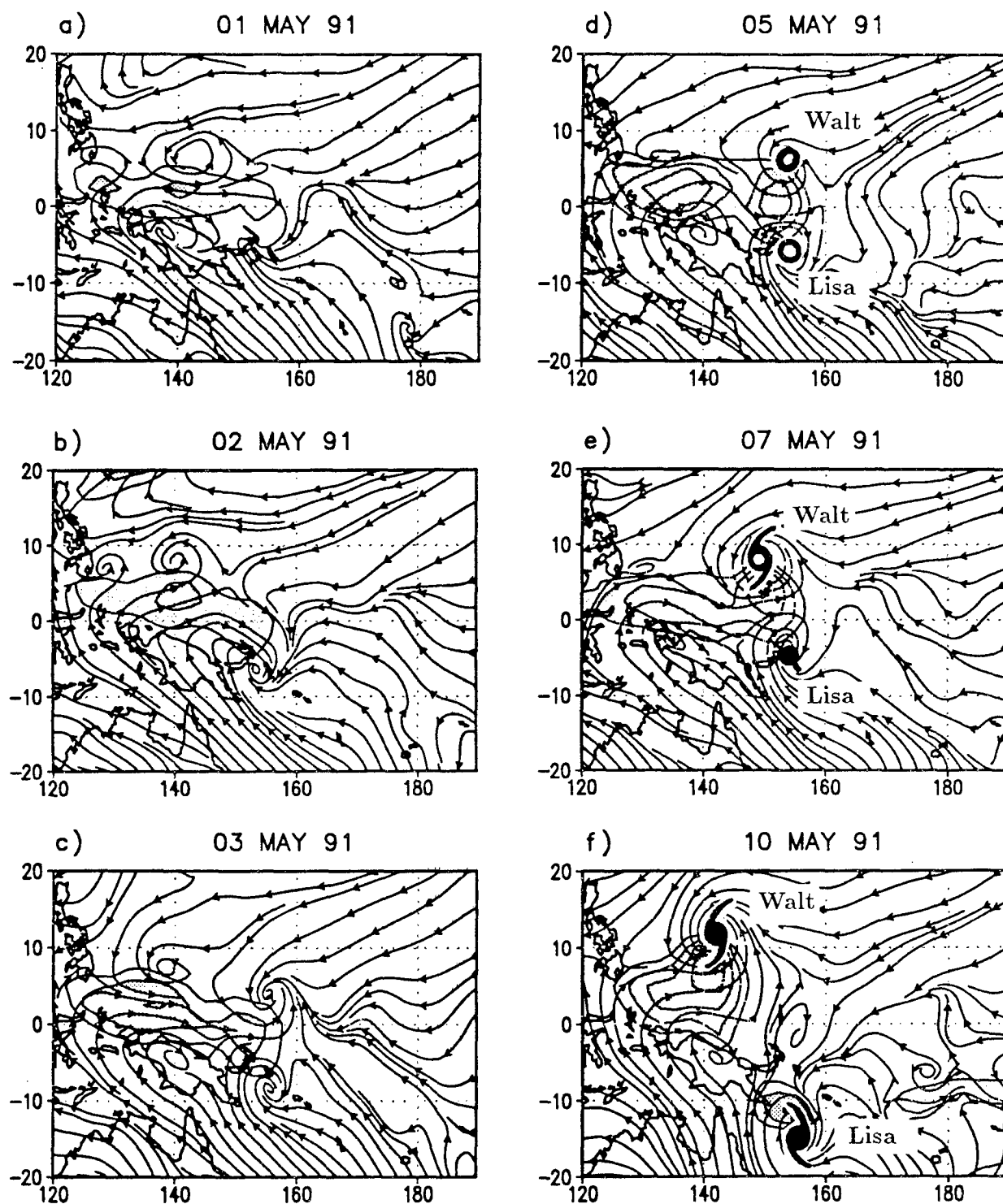
Fig. 15 – Same as Fig. 9, but for a) May 1, 1991, b) May 2, 1991, c) May 3, 1991,
d) May 5, 1991 e) May 7, 1991, f) May 10, 1991

of westerlies is evident at all three latitudes: 2°N, °0, and 2°S. Otherwise, many of the relatively weak westerlies in July through October, 1991 are associated with developing northern hemisphere tropical systems, including Typhoons Amy, Brendan, and Caitlin in July, Typhoon Ivy in early September, Tropical Storm Luke in mid-September, Supertyphoon Mireille from mid- to late September, Typhoons Orchid and Pat in the first half of October and Supertyphoon Ruth in the latter half of October. None of the Northern Hemisphere summer cyclones had Southern Hemisphere counterparts. In most of these cases, the westerlies are not as extensive and not as strong as those events observed during the previous Northern Hemisphere winter and spring. However, there is some indication from the buoy data that NOGAPS slightly underestimated the strength of the westerlies associated with Ivy, Mireille and Ruth (Fig. 8b).

What is notable about the September and early October series of storms is that the point of origin of the initial circulation, as followed over time in NOGAPS, is frequently several degrees south and east of where JTWC locates the initial tropical disturbance. It is often in the early, pre-disturbance, stage of cyclone development that the westerly winds first appear in the equatorial wave guide. By the time a cyclone reaches tropical storm strength and receives an official name, it may have moved a significant distance away from the equator. In these cases, the associated westerly winds may have likewise shifted in position. Thus, attempts to relate named storms to particular observations of near-equatorial westerly winds could be misleading, since isolated data provide an incomplete picture of the spatial and temporal evolution of the events and their connections to one another.

4.4 Late Fall 1991

The largest changes in the eastern equatorial Pacific, associated with the 1991-1992 El Niño, took place in February and March of 1992, as can be seen from the monthly sea surface temperature anomalies shown in Figure 5. Several strong westerly bursts in November, December, and January preceeded these rises. Since the ocean response to these western Pacific wind bursts appears to play a major role in the 1991-1992 El Niño (Kindle and Phoebus, 1994), we will examine the conditions surrounding their development in detail.

In late-October and early November, three tropical systems develop in rapid succession between 5°N and 10°N (Fig. 16a,b). The first, Thelma, forms around 149°E on October 27, but Thelma does not intensify as rapidly or grow as strong as the other cyclone, Seth, which forms around 172°E on October 28. The third cyclone, Verne, is first noted as a tropical disturbance on November 3 at 177°E. All three of these cyclones are accompanied by equatorial westerlies during their early stages of development, and at times, the storms are close enough together that the individual westerly patches merge with one another. However, even though the westerly forcing on the equatorial ocean is extended far to the east as Verne develops, it is of short duration, as these storms move quickly to the west and north.

Of particular interest in this series of analyses are the two easterly waves seen in Figure 16c, one just west of the dateline and the other at the edge of the map near 160°W. Cyclonic circulations develop on these waves over the next couple of days, and those two features will be maintained in the NOGAPS analyses for many days hence. Later in November, these same features will be associated with a major westerly wind burst that persists through the latter half of the month. On November 10 (Fig. 16d) three new cyclones are forming to the east of Seth and Verne, which by now have little influence on the equatorial winds. The wave that was near the dateline three days ago is now the cyclonic circulation near 160°E, while the second wave now appears as a coupled cyclonic circulation around 170°W. The first appearance of equatorial westerlies is between this cyclone couplet, a pattern we have seen often in the past. As in the Russ/Joy case (Fig. 10), over the next few days the westerly patch extends westward, with the maximum wind speeds still between the cyclones (Fig. 16e). However, in this case the westerly expansion is probably aided by the continued westward movement of the first vortex, which is now a
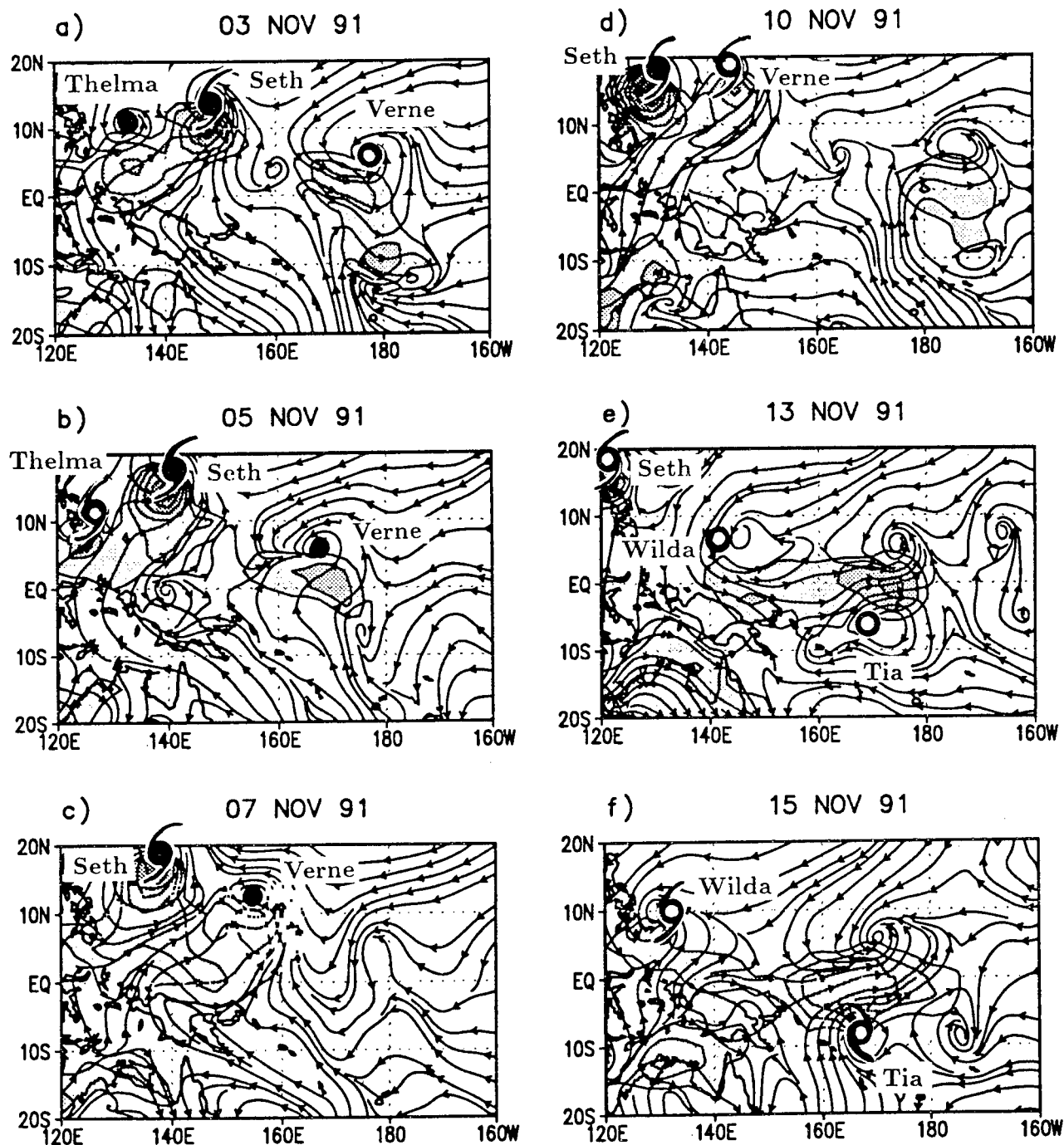
Fig. 16 – Same as Fig. 9, but for a) November 3, 1991, b) November 5, 1991, c) November 7, 1991,
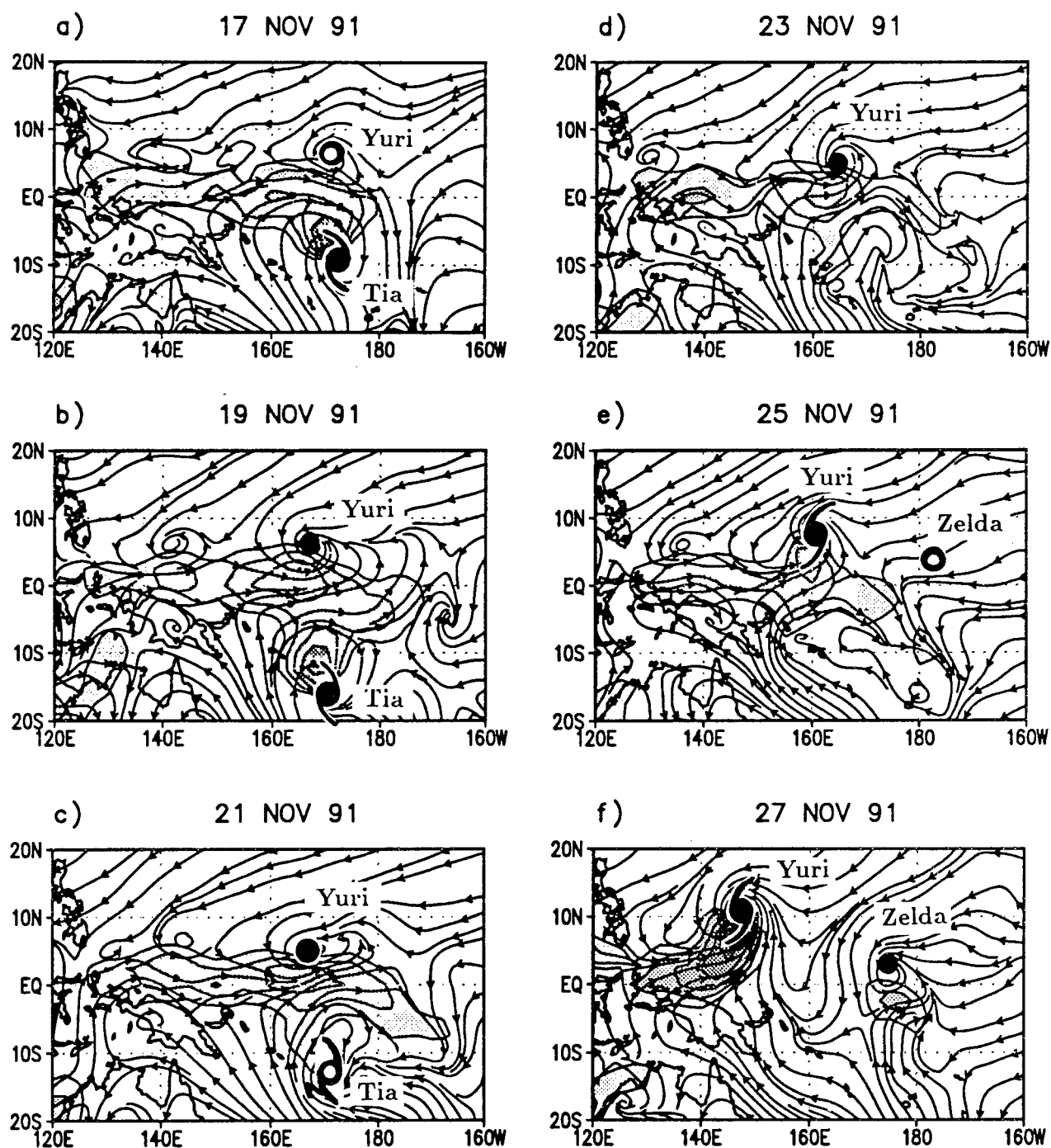d) November 10, 1991, e) November 13, 1991, f) November 15, 1991

Fig. 17 – Same as Fig. 9, but for a) November 17, 1991, b) November 19, 1991, c) November 21, 1991,
d) November 23, 1991, e) November 25, 1991, f) November 27, 1991

tropical disturbance (Wilda) located just east of 140°E. As Wilda continues to develop and track to the northwest, the westerly fetch along the equator lengthens, extending from 135°E to well past the dateline by November 15 (Fig. 16f). During this same period, the westerlies intensify and Tia reaches tropical storm strength in the Southern Hemisphere.

On November 16, JTWC begins tracking an area of deep convection at 5°N, 172°E, near the northern cyclone that has persisted in NOGAPS since November 10. The northern disturbance (Yuri) drifts slowly westward, while Tia intensifies rapidly, reaching Tropical Cyclone (Typhoon) status by 00Z on the 17th (Fig. 17a). As we have seen in other cases, as Tia strengthens and moves away from the equator, the westerly wind speeds also increase, but the wind maximum follows the storm (Fig. 17a,b). Meanwhile, the westerlies have increased south of what is now a tropical depression in the Northern Hemisphere. By November 21, Tia is dissipating, but the westerly fetch along the equator continues to increase and extends well east of the two cyclones (Fig. 17c). However, the tropical depression does not reach tropical storm strength until November 23, by which time the westerly patch has weakened overall, with the strongest winds confined to the region south of Yuri (Fig. 17d). Yuri continues to develop rapidly, reaching typhoon intensity at 18Z on November 24. Typhoon Yuri accelerates as it tracks to the northwest, while the associated band of equatorial westerlies retreats with the storm (Fig. 17e). Also, a new tropical disturbance has formed near 4°N, 182°E and is accompanied by a band of westerlies along its southern inflow region, thus beginning the cycle anew (Fig. 17f). This depression becomes Typhoon Zelda on the 29th.

What is remarkable about this last series of figures is the number of storms that formed near the equator in close succession, resulting in almost continuous westerly forcing on the ocean during the month of November. Furthermore, Supertyphoon Yuri was traced back in the NOGAPS analyses to an easterly wave that was first detected on November 7, 1991--17 days before Yuri became a tropical storm. Prior to the initial insertion of synthetic data for Yuri on 00Z, November 24, NOGAPS analyzed a circulation in the position where the storm initially developed, utilizing only the standard suite of observations that are available to all of the operational centers, plus the SSM/I wind speed observations. The TAO buoy observations were not available in real-time via GTS during this period.

Although the westerlies often appear before the initial tropical disturbance, we have also observed that the larger-scale cyclones are present in the model prior to development of the intial disturbance. In the model, at least, the westerlies are developing in synchronization with the tropical cyclones. Figure 18 illustrates this point by comparing a time series of the zonal and total wind speeds at two single points along the equator to the time lines showing the developmental stages of Verne, Tia, and Yuri. The first burst, which is most evident at 170°E (Fig. 18a), begins on November 3, just as the new tropical disturbance (Verne) is first noted around 177°E. The westerlies increase as Verne progresses to a tropical depression on the 4th and passes to the west of 170°E. As Verne continues to move farther away from 170°E, the westerlies rapidly disappear. The peak in westerly wind speed at 160°E (Fig. 18b) on November 5 is associated with the approach of Verne, and again, the equatorial westerlies decrease as Verne moves north of 10°N and west of 160°E.

The second westerly burst begins on November 10th-11th, as NOGAPS begins to analyze the cyclone couplet just east of the dateline. The wind speeds increase as tropical disturbance Tia forms near 165°E on November 12. Tia reaches tropical storm strength before 00Z on November 14 and moves almost due east until it reaches tropical cyclone strength on the 16th. By that time Tia is just east of 170°E and still north of 10°S and the westerly winds are reaching their peak (Fig. 18a). Tia begins to move almost due south about the same time as the another disturbance (Yuri) develops in the Northern Hemisphere. The westerly winds at 179°E increase again (Fig. 18b) as Yuri drifts slowly westward from its initial position
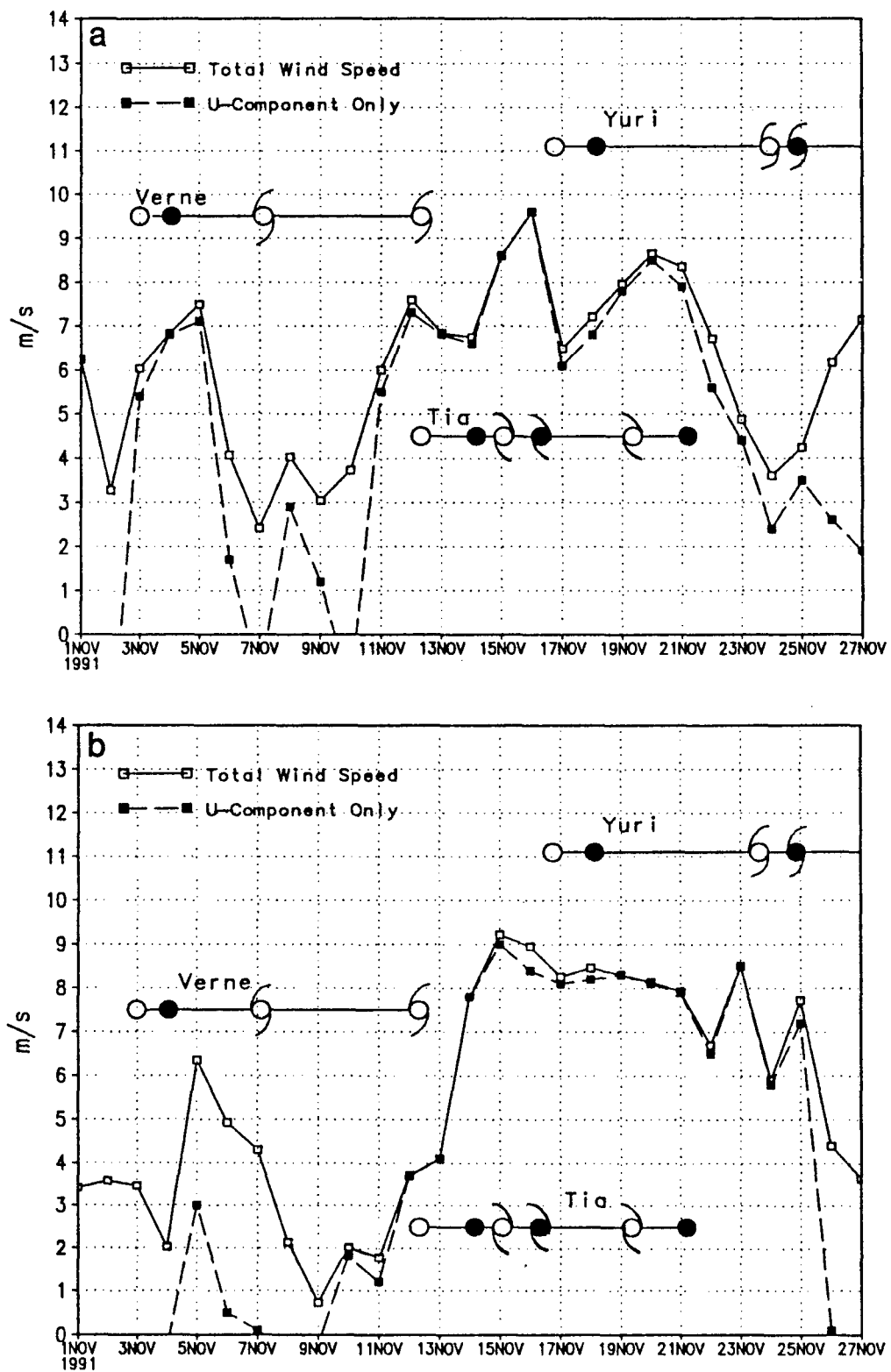
Fig. 18 – Same as Fig. 13, but for points (a) 170°E, 0°N and (b) 160°E, 0°N in November, 1991

near 172°E. Yuri intensifies to a tropical depression on the 18th and finally increases to tropical storm strength on November 23rd. The slow westward motion of Yuri finally results in a decrease in westerly wind strength at 170°E, while at 160°E, the westerlies are sustained throughout the period, with a slight increase on the 23rd and another on the 25th as Typhoon Yuri passes by 160°E. After Yuri's passage, the westerlies disappear altogether.

Figure 19 shows a time series of the wind vectors along the equator in the eastern Indian and western Pacific oceans for the month of November, 1991, with the u-components shaded. Once again, the strongest signal observed is the propagation of the westerly winds from east to west in both the Indian Ocean and the western Pacific, which implies an association with the movement of the tropical cyclones. However, in this case, unlike March 1991, there is some evidence of a signal propagating from the Indian Ocean into the Pacific Ocean as well, particularly if we consider that such a signal might easily be lost as it passes over the Indonesian land masses (100-125°E). A longer time series would be required to definitively pick up such a signal, but we can't rule out the possibility that the westerly burst and associated cyclone activity is enhanced by an intraseasonal oscillation.

In early December, a southerly and easterly cross-equatorial flow is present in the western Pacific, and on December 3, a new cyclone appears in NOGAPS just east of the dateline in the southern hemisphere (Fig. 20a). Westerly winds extend into the central Pacific in the area from 0-10°S. On December 4, the westerly wind speeds increase, with a maximum zonal component of 10 m/s near 5°S, as the southern hemisphere cyclone becomes a tropical depression. Another Southern Hemisphere wave is apparent around 195°E, and westerlies extend to 20°E north of this area, still mostly south of the equator. By December 5 (Fig. 20b), the large fetch of westerlies flows well past the dateline into the center of a new Southern Hemisphere cyclone near 10°S, 160°W. These two Southern Hemisphere circulations develop into Tropical Cyclones Val and Wasa, and analyzed westerlies sometimes reach speeds of 25 m/s. On December 9 (Fig. 20c), the two storms are located within 10 degrees longitude of one another. As Val and Wasa move southeastward away from the equator, the flow across the equator becomes more northwesterly. On December 14, the remnants of Wasa regenerate near 22°S, 150°W to become Tropical Storm Arthur, which tracks northeast before dissipating on the 17th.

As can be seen from Figures 6 and 7, the westerly burst associated with Val and Wasa was much stronger in the Southern Hemisphere than along the equator, where winds were generally from the northwest. However, these two storms are significant in that they formed east of the dateline, a phenomena often observed in El Niño years (Revell and Goulter, 1986), and the associated equatorial westerly anomalies extended much further into the Pacific basin (to 160°W). As described in Keen (1988), the extension of the westerly anomalies into the central Pacific is regarded as an important element in the triggering of El Niño episodes and, as discussed by Kindle and Phoebus (1994), is a key factor in governing the different equatorial ocean responses during the 1990-1991 and 1991-1992 seasons. Further support for this idea is provided by the last series of westerly wind bursts in this study, which occurred as two different Northern/Southern Hemisphere couplets developed near and east of the dateline in January and early February of 1992.
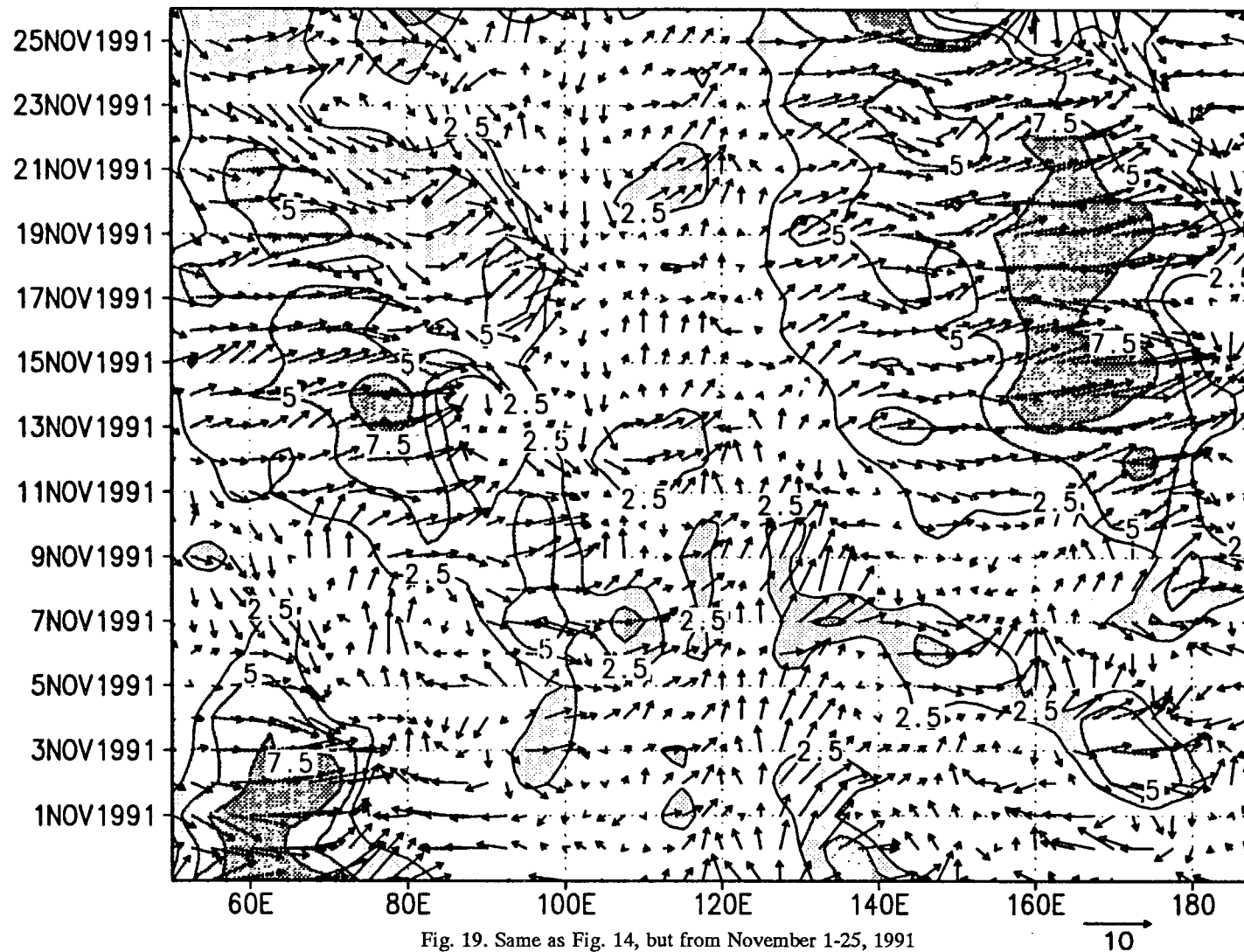
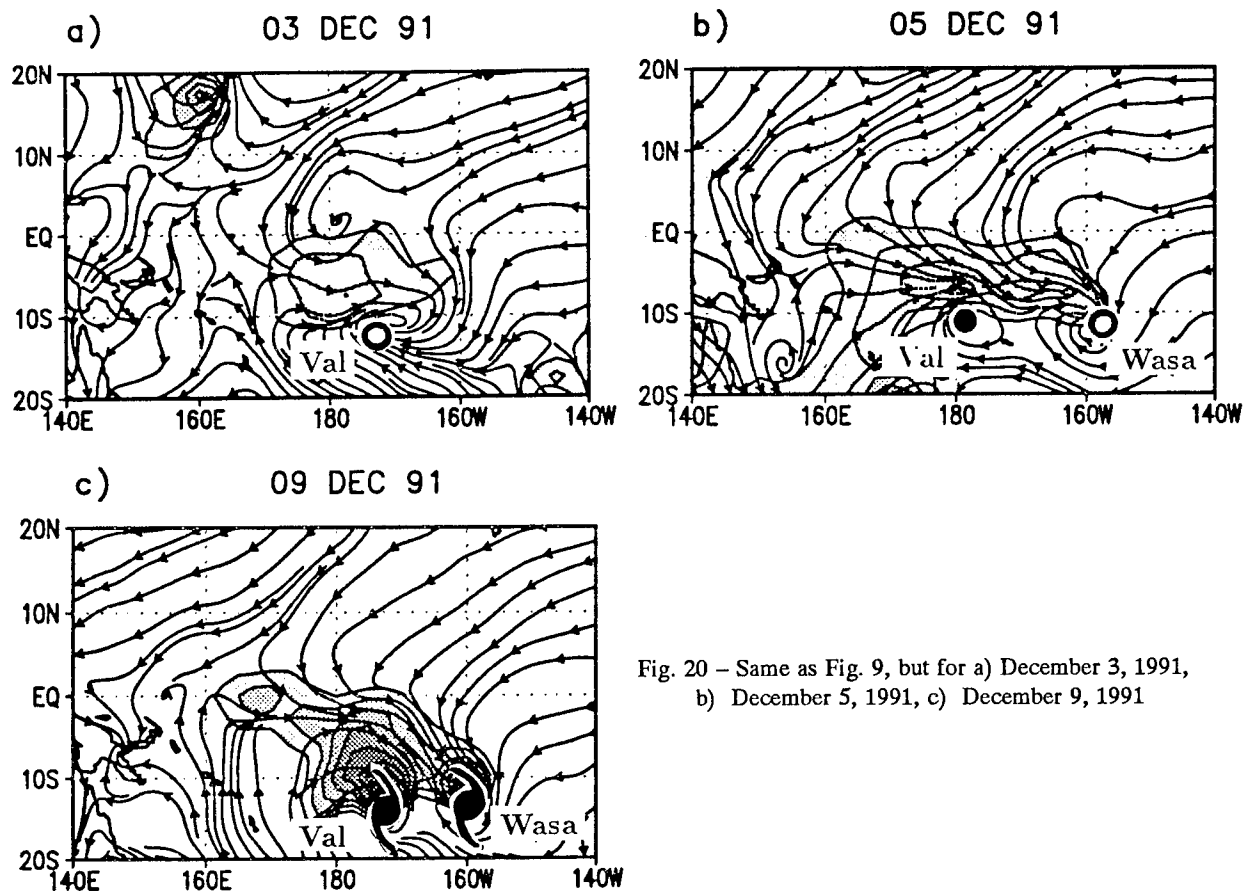Fig. 19. Same as Fig. 14, but from November 1-25, 1991

a) 03 DEC 91

b) 05 DEC 91

c) 09 DEC 91

Fig. 20 – Same as Fig. 9, but for a) December 3, 1991,
b) December 5, 1991, c) December 9, 1991

4.5 Early Winter 1992

The first westerly winds of this next series appeared along the equator in NOGAPS on December 25, at which time there was a weak coupled circulation evident near 170°E in the two near-equatorial troughs (Fig. 21a). The westerlies increase in strength as this couplet moves west and on December 29, the strongest westerlies extend along the equator from 125°E, terminating near the couplet at 160°E. Weaker westerlies are evident in the equatorial waveguide as far east as 175°E, where NOGAPS is beginning to analyze another coupled circulation (Fig. 21b,c). Over the next several days, the zonal component of the wind strengthens and by December 31, westerlies extend from the southern Indian Ocean into the western Pacific. Speeds along the equator continue to increase, and by January 2, exceed 10 m/s. These strong westerlies extend all the way to the dateline, where the second cyclone couplet is now very well-defined (Fig. 21d).

Once again, we have the classical development of a pair of tropical cyclone twins. Axel, in the Northern Hemisphere, develops slightly before Betsy, in the Southern Hemisphere (Fig. 21e). In this case, there appears to have been a true surge in the westerly winds prior to the cyclone development, with higher wind speeds first evident around 140°E and later analyzed further to the east. The strongest westerlies are present between the two cyclones, but do not extend as far to the west as they did earlier. The westerlies continue to increase in strength, however, as the northern storm becomes Typhoon Axel on January 7, followed by Tropical Cyclone Betsy in the Southern Hemisphere on January 8. Another pocket of westerlies south of the equator becomes more prominent as tropical depression Mark forms and moves over the Gulf of Carpentaria.

a) 25 DEC 91

d) 02 JAN 92

b) 27 DEC 91

e) 06 JAN 92

Axel

Betsy

c) 29 DEC 91
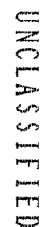
f) 08 JAN 92

Axel

Mark

Betsy

Fig. 21 – Same as Fig. 9, but for a) December 25, 1991, b) December 27, 1991, c) December 29, 1991, d) January 2, 1992, e) January 6, 1992, f) January 8, 1992

As the Axel/Betsy couplet begins to separate, the strongest westerlies are drawn off the equator and the fetch is reduced as the storms also move westward (Fig. 21f). The equatorial westerlies are gradually replaced by easterlies, as we've seen in so many other cases. Some westerlies remain along the equator over the next several days, south of dissipating Typhoon Axel, which doesn't cross north of 10°N until January 12. While the westerly burst associated with the formation of Axel and Betsy was not as long-lived as the burst in November, the January burst provided the strongest equatorial forcing, in terms of zonal wind speed, that we have observed.

In mid-January, the Australian monsoon flow extends into the central South Pacific and shifts northward. By January 16, very zonal westerly winds with speeds approaching 15 m/s extend as far eastward as 165°W, terminating near the point where tropical depression 13P is located (Fig. 22a). By January 18, the depression is upgraded to a tropical storm, and unlike other cases we've observed, this time the maximum winds do not move off the equator with the storm (Fig. 22b). Rather, the strongest westerlies remain well established between the two near-equatorial troughs. By January 23, the Southern Hemisphere westerlies extend well past the dateline (Fig. 22c). NOGAPS begins to form a pair of coupled cyclones in these troughs (Fig. 22d), even as the flow in the western part of the domain is replaced by easterlies.

Although the southern circulation does not develop into a tropical cyclone, the northern cyclone rapidly intensifies to become a rare January hurricane in the central Pacific. Equatorial westerly forcing on the ocean increases as this development occurs (Fig. 22e,f). Hurricane Ekeka spends most of its life south of 10°N, and weakens significantly after it crosses the dateline. The westerlies are soon replaced by weak, disorganized flow all along the equatorial region. A few days later, Tropical Cyclone Cliff forms in the central south Pacific around 10°S, 145°W, even further east than Ekeka.

As we have seen, the end of 1991 into early 1992 was dominated by a series of strong westerly wind bursts along the equator. The event of longest duration was associated with the development of Supertyphoon Yuri, while later bursts were associated with cyclones that developed progressively further to the east. The last storm of the series studied formed well east of the dateline, as did the pair of Southern Hemisphere cyclones in early December. As discussed in Kindle and Phoebus (1994), this series of westerly wind bursts from November to mid-January provided a powerful punch to the equatorial waveguide, resulting in the largest Kelvin wave response during the 1991-1992 El Niño.

5   DISCUSSION

In case after case of model-depicted westerly wind events, the pattern repeated is much the same, with a few exceptions. The majority of the time, the westerlies develop in conjunction with a developing tropical cyclone or cyclone pair. Westerlies first appear as a low-level cyclonic circulation develops on an easterly wave or in one of the shear zones associated with the monsoon or near-equatorial troughs. As the circulation persists, the westerlies become more extensive and increase in speed, often prior to the time the circulation becomes a named tropical storm. As the cyclone intensifies, so do the equatorial westerlies, with the maximum westerly winds analyzed by NOGAPS during the stronger stages of the storm. In the later stages, however, the eastward extent of the westerlies retreats as the tropical cyclones strengthen and move away from the equator. Since the wind maximum also follows the storm, this retreat is often accompanied by decreasing wind speeds along the equator. In the cases where equatorial westerlies are not associated with developing tropical storms, there may still be other low-level circulations observed in the NOGAPS analysis or active convective areas present. In relatively few cases, there are no analyzed cyclones and the westerlies are associated only with strong monsoon flows or the presence of near-equatorial troughs in each hemisphere.

a)   **16 JAN 92**

b)   **18 JAN 92**

c)   **23 JAN 92**

d)   **27 JAN 92**

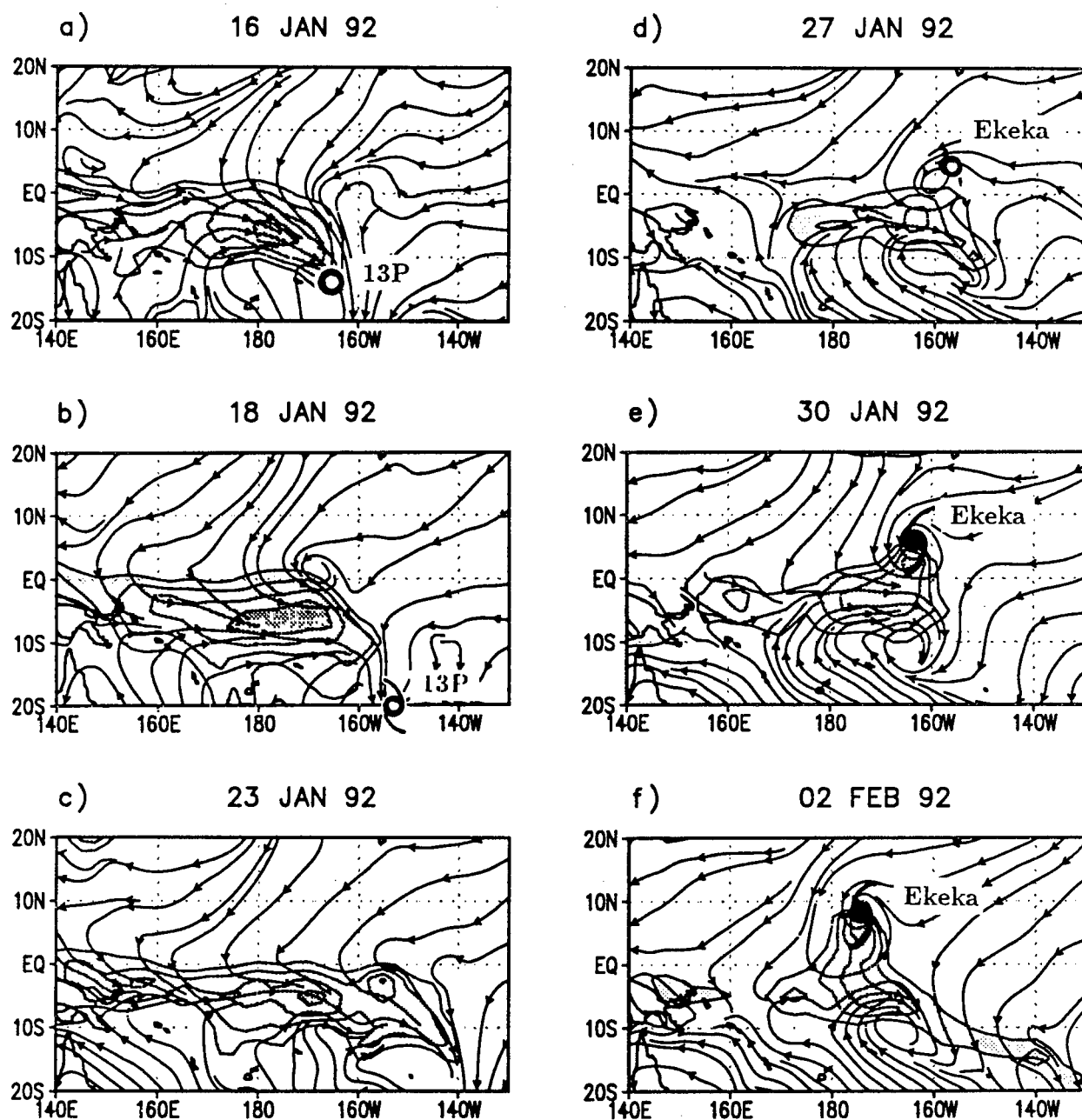**e)**   **30 JAN 92**

f)   **02 FEB 92**

Fig. 22 – Same as Fig. 9, but for a) January 16, 1992, b) January 18, 1992, c) January 23, 1992.
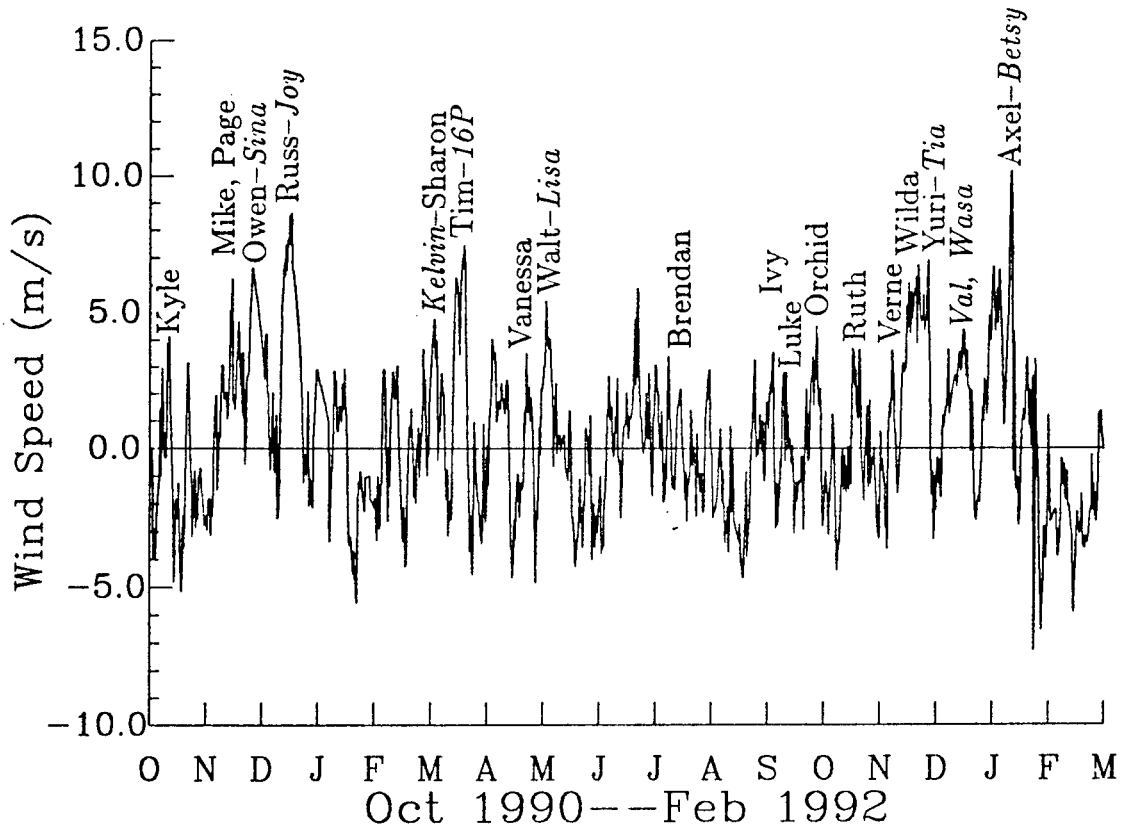d) January 27, 1992, e) January 30, 1992, f) February 2, 1992

Fig. 23 – NOGAPS 10-m zonal wind component at 0°N, 156°E, with a three-day filter applied. Tropical cyclones associated with particular westerly wind bursts are noted, with Southern Hemisphere storms in italics and dual-hemisphere couplets hyphenated.

A time series of the 10-m zonal wind component at 156°E,°0°N is shown in Figure 23, annotated with the names of the tropical systems that were associated with particular westerly events. The correspondence is higher than the 40% association reported by Harrison and Giese (HG; 1991), particularly for cases where the zonal wind component exceeds 3 m/s. All but one of the westerly wind events with zonal wind speeds exceeding 5 m/s are associated with developing tropical cyclones during the period from October 1990 through February 1992. At 3 m/s, the incidence of tropical storms developing in conjunction with WWB is still 89%.

This difference could be a result of several factors. First, of course, our study only encompasses a period of about 1.5 years, while HG used 23.5 years of data. But the standards used to determine an association were also quite different. HG relied on certain predefined criteria: the observed westerly winds at islands near 175°E had to occur within 7 days of a named storm, and the storm had to be located between 20°S-20°N, 160°W-160°E at the time it was named. On the other hand, we determined the association by tracking the vortices over their entire life cycles from series of NOGAPS analyses. In some cases, the initial tropical disturbances and depressions persist for more than 7 days before reaching tropical storm (named) strength. During this early stage, the developing cyclones may change position dramatically, particularly in the east-west direction (Table 3). Thus, a westerly wind observed at 170°E may be associated with a circulation that 8 days later becomes a tropical storm at 140°E. For example, Page was tracked for 17 days before it reached tropical storm strength. During that time, it moved more than 2300 km to the west. Even Vanessa, which was named on the fifth day of its existence, moved over 27 degrees of longitude during those first five days. Large changes in latitude can also take place during the early stages of tropical cyclone development. The latitude range of 20 degrees used by HG is significant only if the tropical storms forming near that latitude spent the earlier part of their existence close to the equator.

Table 3 – Tropical Cyclone Formation Characteristics of Northern Hemisphere Storms Associated with Equatorial Westerlies

	Location Where Formed			Changes From Disturbances to Storm		
Storms	Disturbance Lat, Lon	Tropical Storm Lat, Lon	Typhoon Lat, Lon	Latitude	Longitude	Days Elapsed
Mike	7N, 152E	8N, 144E	9N, 140E	1°	8°	3
Page	8N, 167E	10N, 144E	12N, 138E	2°	23°	17
Owen	7N, 197E	10N, 166E	10N, 165E	3°	31°	8
Russ	4N, 173E	5N, 170E	8N, 159E	1°	3°	2
Sharon	4N, 157E	7N, 146E		3°	11°	5
Tim	3N, 166E	8N, 155E	14N, 153E	5°	11°	4
Vanessa	4N, 145E	12N, 118E		8°	27°	6
Walt	5N, 152E	8N, 150E	11N, 146E	3°	2°	3
Amy	12N, 148E	15N, 134E	18N, 128E	3°	14°	4
Brendan	7N, 153E	17N, 126E	17N, 123E	10°	27°	7
Caitlin	5N, 157E	14N, 132E	19N, 129E	9°	25°	6
Ivy	7N, 165E	9N, 153E	15N, 148E	2°	12°	4
Luke	14N, 148E	18N, 138E		4°	10°	2
Mireille	12N, 172E	14N, 161E	15N, 157E	2°	11°	3
Orchid	13N, 149E	19N, 142E	19N, 134E	6°	7°	4
Pat	8N, 163E	15N, 158E	16N, 152E	7°	5°	5
Ruth	6N, 156E	11N, 143E	13N, 141E	5°	13°	5
Seth	8N, 172E	8N, 157E	13N, 150E	0°	15°	4
Thelma	6N, 149E	13N, 128E		7°	21°	8
Verne	7N, 177E	14N, 154E		7°	23°	5
Wilda	8N, 141E	11N, 129E		3°	12°	3
Yuri	4N, 172E	5N, 166E	7N, 162E	1°	6°	8
Zelda	4N, 182E	8N, 173E	9N, 166E	4°	9°	5
Axel	3N, 176E	6N, 176E	6N, 170E	3°	0°	4
Ekeka	5N, 205E	5N, 202E	6N, 197E	0°	3°	3

Otherwise, it is highly unlikely that storms forming north of 15°N would be associated with equatorial westerlies. In the case of Luke and Orchid, our two northernmost storms, the initial circulations that preceeded the disturbances were even further south than the initial positions shown in Table 3.

While a large percentage of the westerly wind events are associated with named tropical cyclones, Kindle and Phoebus (1994) show that the westerly wind bursts that produce a significant response in the ocean are all associated with tropical storm systems and, in most cases, with tropical cyclone couplets. This result is consistent with the climatology of westerly wind events developed by Keen (1988), which showed that the strongest westerly events were associated with tropical cyclone pairs. Since the ocean response is driven by the surface wind stress, which is proportional to the square of the wind speed, we have computed the zonal component of the wind stress from the 10-m winds using a drag coefficient of 0015. The truly significant westerly wind bursts are highlighted in Figure 24a,b, which compares the surface wind stress along the equator at 156°E to that at 165°E. Bursts producing a stress in excess of 0.05 pascals were associated with tropical cylones in every case but one (a monsoon depression that formed in June, 1991).
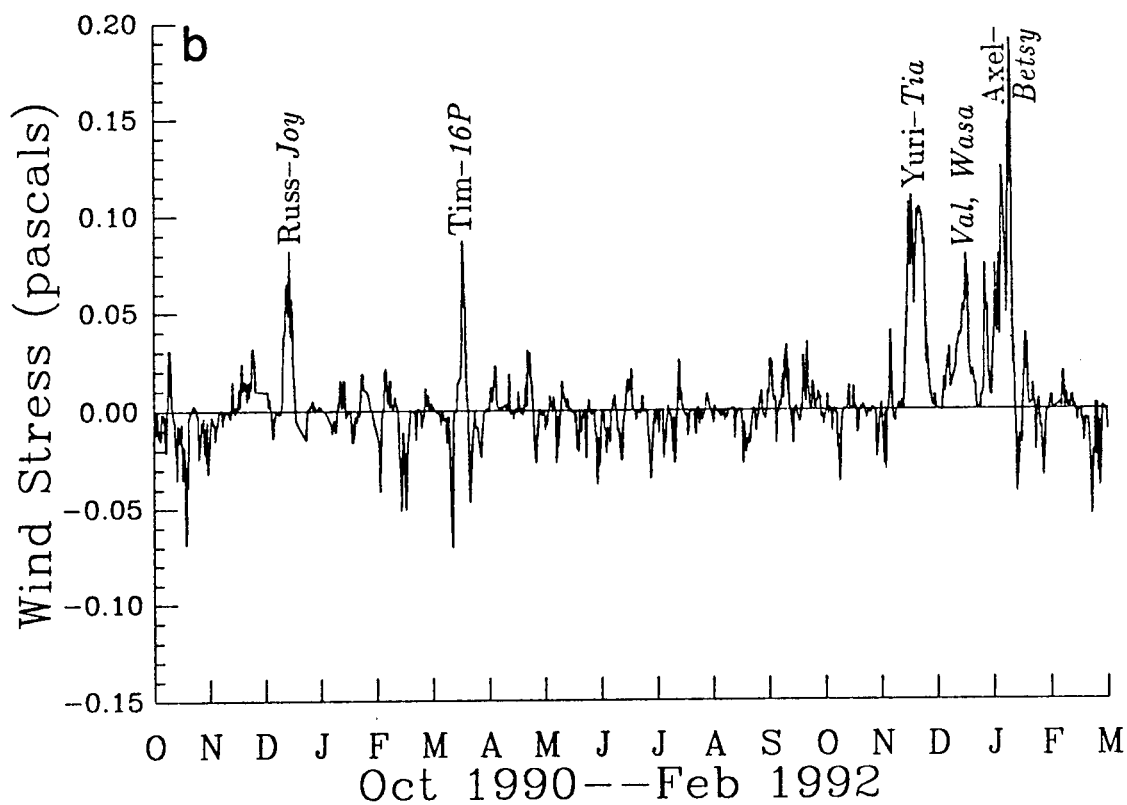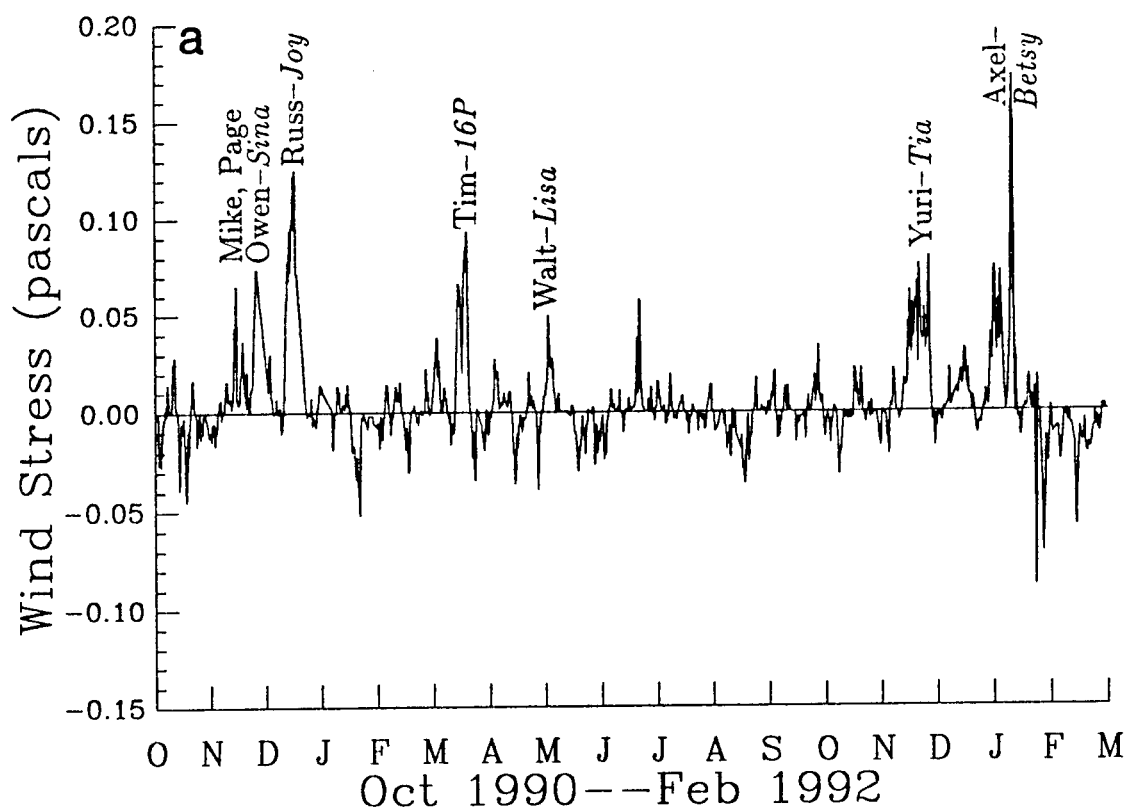
Fig. 24 – Zonal component of the NOGAPS surface wind stress (pascals) at (a) 0°N, 156°E
and (b) 0°N, 165°E, with names of associated tropical cyclones noted

The official points of origin of the tropical cyclones associated with the major bursts in Figure 24 are shown in Figure 25a; Ekeka and Wasa are also included here, even though their influence on the wind field was further east. Interestingly enough, all but one of these storms reached typhoon or supertyphoon strength, and all formed east of 150°E and near the equator, between 15°S and 10°N. If we expand our view and look at the points of origin for all the 1991 western North Pacific storms (Fig. 25b), we see that a large number of them formed east and south. In particular, the storms associated with equatorial westerly wind bursts formed east of 140°E and south of 15°N. Even within this area, the few northernmost and westernmost disturbances were preceded by tropical circulations that in the model fields were initially located east and south of their official point of origin. A similar eastward and equatorward shift in tropical cyclone activity during El Niño years was observed by Revell and Goulter (1986) using South Pacific storm data from 1939 to 1984 and by Chan (1985) using North Pacific storm data from 1948-1982. Interestingly enough, studies that have attempted to correlate the total number of tropical cyclones with ENSO have actually noted a decrease in activity during a major warm event (Solow and Nichols, 1990; Chan, 1985).
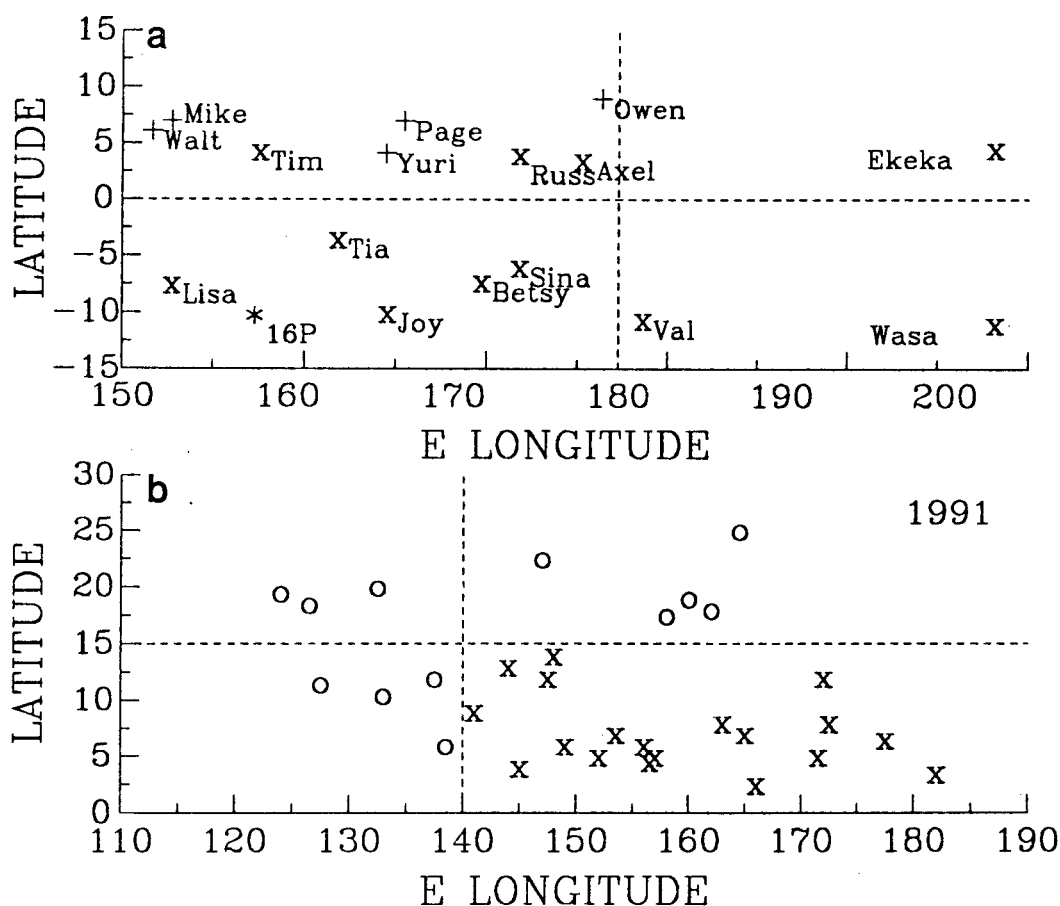
Fig. 25 – Points of origin for (a) the tropical cyclones that were associated with the major westerly wind bursts seen in Fig. 24, and (b) the 1991 northwestern Pacific tropical cyclones. In (a), supertyphoons are indicated with a +, typhoons with an X, and depressions with an *. In (b), tropical cyclones associated with westerly wind bursts are marked with an X.

As part of this study, we looked at storm tracks from the last two decades to determine if the patterns observed in 1991 could be seen in other years. Looking at just the total number of tropical cyclones in the North Pacific (upper curve, Fig. 26), there is no clear relationship between tropical cyclone activity and the El Niño periods (1972-1973, 1976-1977, 1982-1983, 1986-1987, 1991-1992). But, when we include only the number of tropical cyclones that form south of 12°N and east of certain longitudes (lower curves, Fig. 26), a more distinct pattern emerges. Tropical cyclone activity in this region peaks in the years that mark the beginnings of the warm cycles (1972, 1976, 1982, 1986, 1991) and declines during the major cold cycles (1973, 1975, 1984-1985, 1988).

Figure 27a compares the number of Northern Hemisphere cyclones south of 12°N and between 145-180°E directly to the Niño 3 SST anomaly index from the eastern equatorial Pacific. There is a striking similarity in these two curves. Even the moderately warm period from late 1978-1980 is reflected by a relatively higher level of western Pacific cyclone activity in this region, while the increase in SST anomalies in early 1974 could also be related to the less significant peak in tropical storm activity that is present at that time. The maximum warming in the Niño 3 area occurs in the latter quarters of 1972, 1976, and 1982; in the first month of 1992; and in the third quarter of 1987. Thus, in each instance, the eastward and equatorward shift in tropical storm activity in the western North Pacific occurs prior to the peak warming in the eastern Pacific.
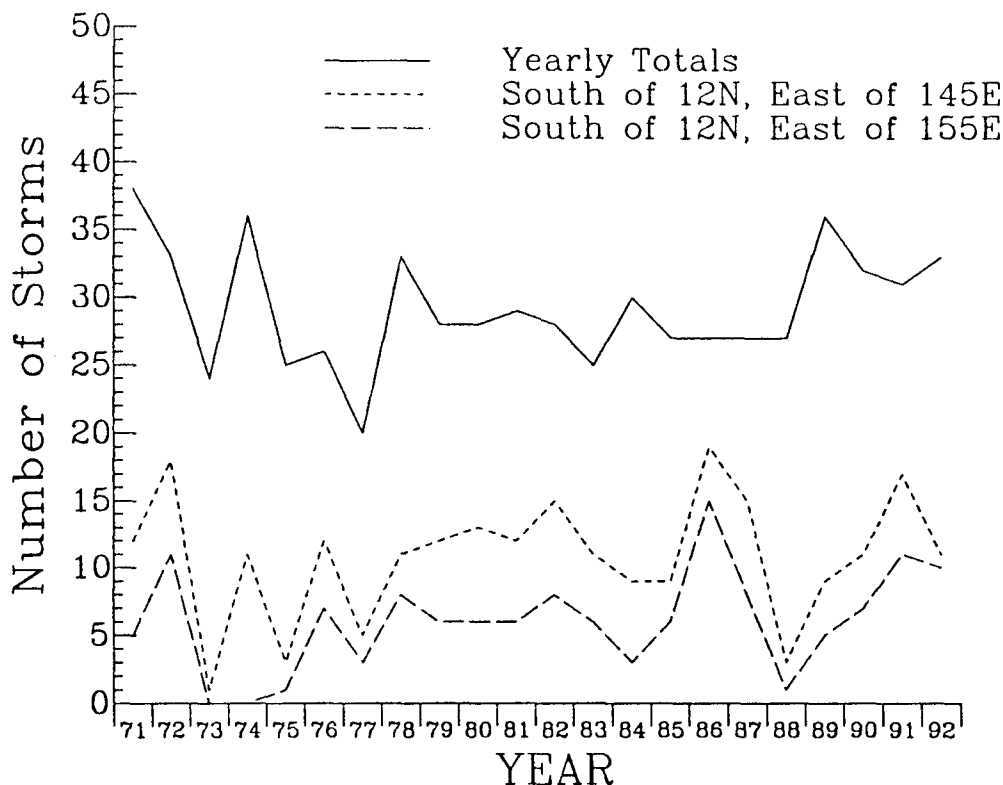

Fig. 26 – Number of western Pacific tropical cyclones, by year, that formed in particular areas, compared to the total number for the year, as tracked by JTWC
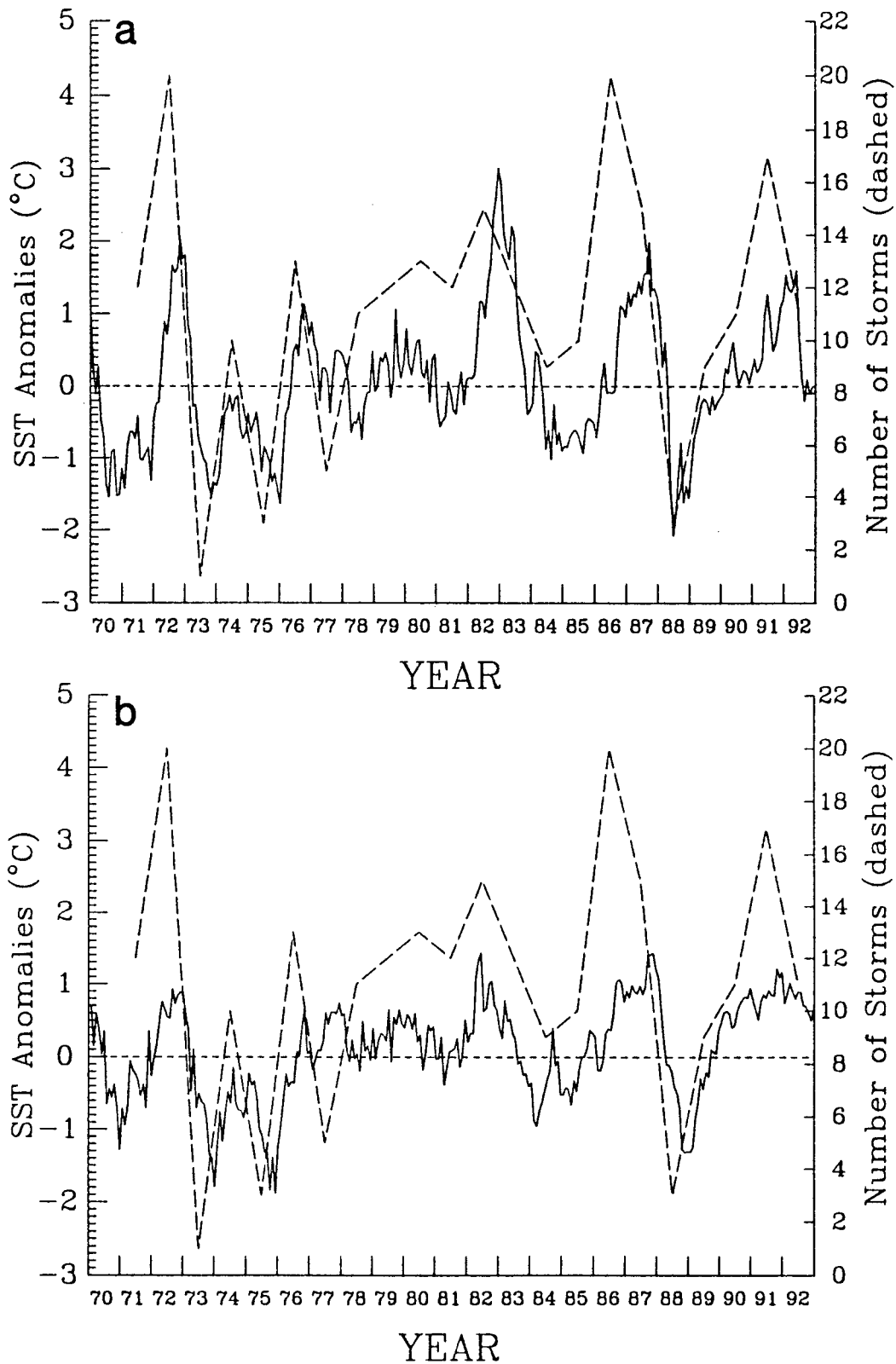
Fig. 27 – (a) Monthly sea-surface temperature anomalies in the Niño 3 region (solid curve) compared to the annual number of tropical cyclones tracked by JTWC between 0°-12°N and 145°-180°E (dashed curve). (b) Same as (a), but for the Niño 4 region in the central Pacific.

Generally, the shift in tropical storm locations occurs in the years when the central Pacific SST anomaly is becoming increasingly positive (Fig. 27b) but, with the exception of 1982, has not yet reached a maximum. Table 4 shows that during these years, the development of tropical cyclones in the area bounded by 0-12°N and 145-180°E occurs throughout the year, in nearly every month, with clusters in the latter half of 1972, 1986, and 1991 and the middle of 1982. It is possible that these clusters are related to the warmer SSTs. On the other hand, in 1976 the SST anomaly didn't become positive until late in the year, but a substantial number of tropical cyclones formed early in the year while negative SST anomalies were present in the central Pacific. However, we hesitate to draw any conclusions from this comparison, since the Niño 4 index covers an area that only partially coincides with the region of cyclone formation. That aside, our primary interest is still in the ocean response to the shifts in tropical cyclone formation patterns and the associated equatorial westerlies.

Table 4 – Monthly Distribution of Tropical Disturbances that Formed in the Area from 0-12°N, 145-180°E, as Tracked by the JTWC in Guam

	1972	1976	1982	1986	1991
January	1	1	0	0	0
February	0	1	0	1	0
March	1	0	3	0	2
April	0	1	0	1	1
May	1	1	1	1	1
June	2	1	1	1	0
July	3	2	3	2	3
August	2	1	3	1	0
September	2	2	1	2	2
October	2	1	2	3	3
November	2	1	1	4	5
December	1	0	0	3	0

If we assume, based on the data from 1991, that most of the tropical cyclones forming near the equator east of 145°E in the western Pacific were accompanied by westerly winds in the equatorial waveguide, we can argue for a plausible connection between western equatorial Pacific wind anomalies and eastern equatorial Pacific warming. However, we do not argue that each of these tropical cyclones will have an impact on the eastern Pacific ocean. Easterly wind stress forcing in the central and eastern Pacific certainly may counteract the initial downwelling pulse. But we do believe that an increase in the number of storms or the frequency of storms near the equator and near the dateline increases the probability of strong westerly forcing on the equatorial ocean which, through the generation of equatorially trapped Kelvin waves and anomalous easterwardly currents, increases the likelihood that ocean temperatures will rise in the central and eastern tropical Pacific Ocean. Given the sparse observational network and the absence of accurate model data until fairly recently, the tropical cyclone records may provide another source of data that can be used to infer the presence of westerly winds in the equatorial waveguide.

What is not clear from this study is whether the warm ENSO cycle can be explained entirely by a properly timed series of westerly wind events, as proposed by Keen (1982) and Ramage (1986), or whether the large increase in SST is due to westerly wind forcing superimposed on some longer wavelength signal. Since we have concentrated only on the synoptic-scale events, we cannot address the

nature of the longer-scale signals. However, in the follow-on study we have observed that a sequence of storms, successively developing eastward of the previous storm(s) a month or so later, could account for much of the anomalous warming in the eastern Pacific (see Kindle and Phoebus, 1994). Similarly, the absence of such a scenario could account for the failure of an anticipated El Niño to appear, as was the case in 1990-1991.

One difference that is evident between the Northern Hemisphere winters of 1990-1991 and 1991-1992 is that in the former, following the Russ/Joy cyclone couplet in December, 1990, no other storms developed until March, 1991, when the Sharon/Kelvin couplet formed. However, during the latter season, the tropical storms and their associated westerly wind bursts appeared in October, and at least one major storm developed near the equator in each succeeding month, up to and including February, 1992. Several, but not all, of these storms were coupled with Southern Hemisphere cyclones. We also observed an eastward shift in development, with the early signs of Yuri (November 1991) first seen around 170°W, and Val and Wasa (December 1991) forming in the Southern Hemisphere east of the dateline. The December-January couplet, Axel and Betsy, developed near 170°E, followed by another coupled cyclone pair around 200°E that produced Ekeka in late January/early February. In late 1990, no storms formed east of the dateline. This eastward shift is also reflected in Figure 24. The surface wind stress at 165°E is dominated by the westerly bursts during the latter part of 1991 and early 1992, whereas the zonal wind stress at 156°E is strong in both late 1991 and late 1990.

Another noticeable difference between the two seasons is that even though Supertyphoons Mike, Page, and Owen produced strong westerlies, they generally developed further north than Yuri, Axel, and Ekeka. Furthermore, Owen was the only storm in the first series that had a Southern Hemisphere counterpart. Table 3 summarizes the pattern of development of the westerly wind burst storms by giving the approximate latitudes of the initial disturbance, the initial tropical storm, and its position when upgraded to a typhoon, if that occurred. The storms associated with the strongest westerly bursts are shown in bold-face type. Note that they all became tropical storms before moving north of 10°N, while few of the storms associated with the weaker events did. Furthermore, the storms preceeding the 1991-1992 El Niño reached typhoon stage while still located very near the equator. Thus, the major westerly wind bursts at the end of 1990 were not only confined further to the west, but they were not as concentrated along the equator as those associated with the 1991-1992 fall and winter seasons' storms.

While we have shown that there is a clear association between tropical cyclone activity and equatorial westerly wind events in the western Pacific, the exact nature of this relationship is still uncertain and will require a more in-depth study than we have performed so far. The key question to be answered is whether (1) the westerlies are a product of the developing cyclones, (2) the cyclones develop in response to the westerly bursts, (3) both events are generated by some other mechanism, or (4) some combination of all these things is occurring. It is fairly straightforward to make a case for the development of tropical systems by the westerly wind bursts, since the area of low-level convergence between the westerlies and the easterly trade winds would be a prime location for tropical cyclone formation. This area defines the region of ascending motion between the zonal circulation cells, with strong divergence in the upper levels (Heta, 1991). Furthermore, the deflected westerlies will increase the positive vorticity in the lower levels (Ogura and Chin, 1987).

Some studies have indicated that the initial westerly wind burst is forced by mid-latitude cold surges, which raise the sea-level pressure in the western Pacific, resulting in a down-pressure gradient acceleration of the wind to the east (Lim and Chang, 1981). Of course, if a tropical cyclone begins to develop near the eastern edge of these westerlies, the pressure drop associated with the developing storm would further enhance and prolong the westerly wind burst. This scenario was observed by Chu and Frederick (1990) from their case study of a May 1982 burst.

However, in the model fields, the initial westerlies often appear simultaneously with the initial cyclonic circulation on the easterly wave, and both features appear to develop and strengthen in conjuction with one another. While we have not included model or satellite convective fields in this study, it is well known that easterly waves are often regions of active convection. Thus, the development of the westerlies may be in response to this near-equatorial heat source. Enhanced westerly inflow could, in turn, contribute to increased convection, setting up a cooperative interaction that may eventually lead to the development of one or more strong, organized tropical cyclones. Model simulations have shown that as the atmosphere attempts to balance the large-scale circulation to an equatorial heat source, an easterly inflow indicative of a Kelvin wave structure develops to the east of the convection, with a strong cyclonically curved westerly inflow present to the west, characteristic of a Rossby wave (Lau et al., 1989). The Rossby wave signature is later evident as a dual-hemisphere cyclone couplet that propagates westward, much as we have seen in the NOGAPS model fields.

Several authors have shown a relationship between tropical cyclone couplets, the appearance of westerly anomalies in the western Pacific, and the 30-to-60 day oscillation (Sui and Lau, 1992; Lau, et al., 1989). This scenario involves a number of multiscale interactions, where super cloud clusters propagate from west to east with the intraseasonal oscillation (ISO), while individual convective areas, such as tropical cyclones, propagate east to west. Although we have not directly observed propagation of westerly winds from the Indian Ocean into the Pacific in each case, there was some indication of an ISO in November, 1991, when the strong WWB in the western Pacific was preceeded by strong westerlies in the Indian Ocean. Some of this signal appears to be lost over the Indonesian land masses, where it is known that NOGAPS and other models have problems accurately representing convection (Fiorino et al., 1993b). We have also observed the successive eastward development of a number of tropical storms during late 1991-1992, each about a month apart, which could be the result of enhanced convection due to eastwardly propagating 30-60 day oscillations.

Many of the efforts to identify the controlling factors for the quasi-periodic nature of the El Niño have focused on the ocean. Under these scenarios, changes in the atmosphere would be in response to changes in the ocean. For example, the equatorward shift in tropical storm formation would result as sea surface temperatures increased in the western Pacific. Then, as the warmer ocean temperatures propagated eastward, tropical storm activity and the westerly wind bursts would also shift further eastward. While it would be interesting to investigate the relationship between SST and individual cyclones more fully, we must note that sea surface temperatures in the western Pacific are almost always above the threshold for tropical cyclone development, and that cyclone development is not governed entirely by near-surface characteristics. Thus, SST changes, in isolation, cannot account for the dramatic shifts in tropical cyclone activity. Upper-atmospheric conditions must also play a role.

In a recent study, Gray et al. (1992) proposed that changes in vertical wind shear, static stability and horizontal wind ventilation associated with easterly anomalies in the stratospheric Quasi-Bienniel Oscillation (QBO) enhance deep convective activity near the equator and supress such activity farther from the equator. This theory is compatible with the shifts we have observed in western Pacific tropical cyclone activity preceeding the major warm events. Kuma (1990) noted a tendency for stronger 30-to-60 day oscillations during the easterly phase of the stratospheric QBO, which suggests a means of relating these two phenomena. The empirical evidence for a QBO-related ENSO cycle is compelling. The approximately 28-month cycle of the QBO, modified by the time required to replenish the western Pacific warm pool, could explain the quasi-periodic appearance of the El Niño, perhaps through enhanced 30-to-60 day oscillations, resulting in stronger, more frequent near-equatorial tropical cyclones and associated westerly wind bursts. These features, in turn, generate eastwardly propagating, downwelling Kelvin waves and anomalous currents in the tropical ocean that result in significant changes to sea surface height and SST

in the central and eastern equatorial Pacific. Thus, more studies on the possible role of multiscale interactions in the atmosphere modulating the ENSO cycle should be encouraged.

6 SUMMARY

This study used low-level wind fields from an operational global data assimilation system to show a strong association between equatorial westerly wind bursts in the western Pacific and developing tropical cyclones in the same area. Because the area of interest is a data-sparse region, and because the spatial extent of the westerly burst may cover only a few degrees of latitude, these events may not be detected by the conventional observations. In this sense, model output provides an important source of additional information, with the advantage that the model-depicted fields are spatially and temporally continuous and dynamically consistent.

In most westerly events, the westerlies first appear as a new cyclonic circulation forms on an easterly wave or in a near-equatorial trough. In the early stages of cyclone development, prior to the appearance of an official tropical depression, the winds become stronger and the zonal wind fetch extends westward. The circulation may also move westward or northward during this time, or it may remain fairly stationary. Whichever the case, the inflow region around the southeastern flank of the cyclone generally marks the easternmost extension of the westerly winds. The peak of the equatorial westerlies is reached before the cyclone begins a significant move away from the equator. As the cyclone develops into a tropical storm or typhoon, it generally tracks initially to the west or northwest (in the Northern Hemisphere). At this point, although the westerly wind speeds continue to increase, the movement of the storm results in a westward and poleward retreat of the zonal winds along the equator. Thus, the fetch is often reduced as the cyclone strengthens, as is the forcing on the equatorial ocean. Eventually, the storm moves far enough away from the equator or far enough west that westerlies are no longer present over the equatorial ocean. These results suggest that the relationship between westerly wind bursts and tropical cyclone formation is one of cooperative interaction. Convection on or near the equator serves to intensify the westerlies, while the increased westerly wind speeds intensify and organize the convection.

The lifetime of a westerly burst is of the order of 1-2 weeks. It generally encompasses about 10 degrees of latitude and 25 degrees of longitude, with peak zonal wind speed reaching 10 m/s. The strongest events may extend from 30 to 50 degrees of longitude, with zonal wind speeds approaching 15 m/s. However, there is a substantial amount of variation between individual events. Sometimes new tropical cyclones form in rapid succession, producing clusters of bursts that result in anomalous westerly forcing on the equatorial ocean that can persist for several weeks.

Not all incidents of westerly equatorial winds will produce a significant response in the ocean. From this study, we determined that the strongest bursts are related to individual tropical cyclones developing at very low latitudes and to dual-hemisphere tropical cyclone couplets, which concentrate the zonal winds into a narrow band right along the equator. All but one of the cyclones associated with significant equatorial westerlies developed into typhoons (tropical cyclones in the Southern Hemisphere), with many of the Northern Hemisphere storms even reaching supertyphoon strength. Thus, regardless of the particular cause/effect relationship between tropical storms and westerly wind bursts, the formation of a tropical storm or typhoon near the equator may be an important ingredient in generating westerly winds that are strong enough and last long enough to force a remote response in the eastern Pacific Ocean.

All of the storms associated with equatorial westerlies from October, 1990 through January, 1992 formed between 15°S and 15°N and east of 140°E. However, the most significant bursts were associated with northern hemisphere storms that formed south of 10°N and east of 150°E, tracked almost due west, and developed into tropical storms or typhoons while still south of 10°N, usually accompanied by a

Southern Hemisphere counterpart. By comparing two decades of western Pacific tropical storm track data to changes in eastern Pacific SST, we confirmed previous studies that indicated a dramatic equatorward and eastward shift occurs in the area of tropical cyclone development during El Niño years. Furthermore, we showed that the peaks of activity near the equator and closer to the dateline often preceed the increased SST in the far eastern Pacific Ocean.

A series of westerly wind bursts along the equator in late 1990 were associated with the development of Supertyphoons Mike, Page, and Owen in November, followed by the Russ/Joy couplet that formed around 170°E in December. While strong westerly winds were present along the equator in each case, they were confined more to the western part of the basin. Only the December, 1990 burst was associated with a strong westerly wind stress at 165°E. The El Niño anticipated during the 1990-91 winter/spring season failed to appear. On the other hand, late 1991 into early 1992 was highlighted by a series of strong equatorial westerlies associated with typhoons that formed successively further east about one month apart-- Yuri/Sina near 165°E in late November, Axel/Betsy near 175°E in early January, and Ekeka near 200°E in late January. Each of these storms evolved from dual-hemisphere coupled cyclones in flow patterns reminiscent of the classical Rossby wave response to an equatorial heat source, and given the time separation between the events, their formation may be due, in part, to convection enhanced by eastwardly propagating intraseasonal oscillations.

If synoptic-scale atmospheric events, such as tropical cyclones and westerly wind bursts, play a role in the El Niño, either as triggering or feedback mechanisms, then it is important to perform coupled air/ocean modeling experiments using an atmospheric model that can simulate tropical storm formation. Unfortunately, for now, most of these experiments will have to be historical in nature, since climate drift problems associated with the general circulation models make long-term coupled forecasting with such complex models unlikely in the near future. However, it is still informative to integrate an ocean model forward in time to predict the ocean response to a particular westerly wind event, with or without continuous atmospheric forcing, as reported by Kindle and Phoebus (1994).

Future plans at the Naval Research Laboratory include performing a reanalysis of the atmospheric data from 1985 to present using the operational global data assimilation system. This effort will allow us to capture another complete El Niño/La Niña cycle. Such a dataset will be extremely useful for in-depth studies of multiscale interactions in the tropics using the full suite of model output products, so that some of the questions posed in this report can be studied more fully. Furthermore, this dataset will provide the ocean modeling community with a longer term, more consistent set of marine winds for driving ocean circulation models.

ACKNOWLEDGMENTS

REFERENCES

Barber, R., and F. Chavez, "Biological consequences of El Niño," *Science* **222**, 1203-1210 (1983).

Baker, N., "Quality control for the Navy operational atmospheric database," *Wea. and Forecasting* **7**, 250-261 (1992).

Barker, E., "The design of the Navy's multivariate optimum interpolation analysis," *Wea. and Forecasting* **7**, 220-231 (1992).

Chan, J., "Tropical cyclone activity in the Northwest Pacific in relation to the El Niño/Southern Oscillation phenomenon," *Mon. Wea. Rev.* **113**, 599-606 (1985).

Chu, P.-S., and J. Frederick, "Westerly wind bursts and surface heat fluxes in the equatorial western Pacific in May 1982," *J. Met. Soc. Japan* **68**, 523-537 (1990).

Chu, P., J. Frederick, and A. Nash,"Exploratory analysis of surface winds in the equatorial western Pacific and El Niño," *J. Clim.* **4**, 1087-1102 (1991).

Clancy, R. M., J. Harding, K. Pollak, and P. May,"Quantification of improvements in an operational global-scale ocean thermal analysis system," *J. Atmos. Ocean. Tech.* **9**, 55-66 (1992).

Clancy, R. M., P. Phoebus, and K. Pollak,"An operational global-scale ocean thermal analysis system," *J. Atmos. Ocean. Tech.* **7**, 233-254 (1990).

Fiji Meteorological Service, "Cyclones of the Southeast Pacific Ocean, 1990-1992," *Mariners Weather Log*, 54-56 (Fall 1992).

Fiorino, M., J. Goerss, J. Jensen, and E. Harrison,"An evaluation of the real-time tropical cyclone forecast skill of the Navy Operational Global Atmospheric Prediction System in the western North Pacific," *Wea. and Forecasting* **8**, 3-24 (1993).

Fiorino, M., S. Lord, W. Lau, P. Phoebus, and C. Strey. "A synoptic-scale overview of the TOGA-COARE Intensive Observing Period November 1992-February 1993 based on analysis from the U. S. operational global data assimilation systems," NASA Goddard Space Flight Center Technical Memorandum 104593, Greenbelt, MD, Nov. 1993.

Giese, B., and D. Harrison, "Aspects of the Kelvin wave response to episodic wind forcing," *J. Geophys. Res.* **95**, 7289-7312 (1990).

Goerss, J., "Evaluation of NOGAPS tropical cyclone forecasting performance for 1991," presented at the 1992 EGPACOM Tropical Cyclone Conference, Tokyo, Japan, 1992.

Goerss, J.,"The impact of bogus observations upon the Navy Operational Global Atmospheric Prediction System," Proceedings of the AMS Twelfth Conference on Weather Analysis and Forecasting, American Meteorological Society, Monterey CA, Oct. 1989, pp. 41-45.

Goerss, J. and P. Phoebus,"The multivariate optimum interpolation analysis of meteorological data at the Fleet Numerical Oceanography Center," Naval Research Laboratory Report NRL/FR/7531--92-9413, Washington D.C., Apr. 1993.

Goerss, J. and P. Phoebus, "The Navy's operational atmospheric analysis," *Wea. and Forecasting* **7**, 232-249 (1992).

Goerss, J., L. Brody, and R. Jeffries, "Assimilation of tropical cyclone observations into the Navy Operational Global Atmospheric Prediction System," Proceedings of the AMS Ninth Conference on Numerical Weather Prediction, American Meteorological Society, Denver CO, Oct. 1991, 638-641.

Graham, N. and W. White, "The El Niño cycle:A natural oscillator of the Pacific Ocean-atmosphere system," *Science* **240**, 1293-1302 (1988).

Gray, W., "Atlantic seasonal hurricane frequency, Part I: El Niño and 30 mb quasi-biennial oscillation influences," Mon. Wea. Rev. **112**, 1649-1668. (1984).

Gray, W., J. Sheaffer, and J. Knaff, "A mechanism for the modulation of ENSO variability by the stratospheric QBO," *J. Meteor. Soc. Japan* **70**, 975-994 (1992).

Harrison, D., and B. Giese, "Episodes of surface westerly winds as observed from islands in the western tropical Pacific," *J. Geophys. Res.* **96** (Supplement), 3221-3237 (1991).

Heta, Y., "The origin of tropical disturbances in the equatorial Pacific," *J. Meteor. Soc. Japan* **69**, 337-351 (1991).

Heta, Y., "An analysis of tropical wind fields in relation to typhoon formation over the western Pacific," *J. Meteor. Soc. Japan* **68**, 65-76 (1990).

Hodur, R. and S. Burk, "The Fleet Numerical Weather Central tropical cyclone model: comparison of cyclic and one-way interactive boundary conditions," *Mon. Wea. Rev.* **106**, 1665-1671 (1978).

Hogan, T. and L. Brody, "Sensitivity studies of the Navy's global forecast model parameterizations and evaluation of improvements to NOGAPS," *Mon. Wea. Rev.* **121** (8), pp. 2373-2395 (1993).

Hogan, T. and T. Rosmond, "The description of the Navy Operational Global Atmospheric Prediction System's Spectral Forecast Model," *Mon. Wea. Rev.* **119**, 1786-1815 (1991).

Hogan, T., T. Rosmond, and R. Gelaro, "The NOGAPS Forecast Model: A Technical Description," Naval Oceanographic and Atmospheric Research Laboratory Report 13, Naval Research Laboratory, Stennis Space Center, MS (1991).

Joint Typhoon Warning Center, "1992 Annual Tropical Cyclone Report," U. S. Naval Meteorology and Oceanography Command Center, Guam, 1993.

Joint Typhoon Warning Center, "1991 Annual Tropical Cyclone Report," U. S. Naval Meteorology and Oceanography Command Center, Guam, 1992.

Joint Typhoon Warning Center, "1990 Annual Tropical Cyclone Report," U. S. Naval Meteorology and Oceanography Command Center, Guam, 1991.

Keen, R. A., "Equatorial westerlies and the Southern Oscillation," Proceedings of the U.S. TOGA western Pacific air-sea interaction workshop, Honolulu, Hawaii, 1988. U.S. TOGA Report No. 8, UCAR, Boulder, CO.

Keen, R. A., "The role of cross-equatorial tropical cyclone pairs in the Southern Oscillation." *Mon. Wea. Rev.* **110**, 1405-1416 (1982).

Kindle, J. and P. Phoebus, "The ocean response to operational westerly wind bursts preceding the 1992-1992 El Niño," *J. Geophys. Res.*, in press (1994).

Kuma, K., "A quasi-biennial oscillation in the intensity of the intra-seasonal oscillation." *Int. J. of Climatology* **10**, 263-278 (1990).

Lander, M. A., "Evolution of the cloud pattern during the formation of tropical cyclone twins symmetrical with respect to the equator," *Mon. Wea. Rev.* **118**, 1194-1202 (1990).

Lau, K.-M., L. Peng, C. Sui, and T. Nakazawa, "Super cloud clusters, westerly wind burst, 30-60 day oscillations and ENSO:A unified view," *J. Meteor. Soc. Japan* **67**, 205-219, (1989).

Lim, H. and C.-P. Chang, "A theory for midlatitude forcing of tropical motions during winter monsoon," *J. Atmos. Sci.* **38**, 2377-2392 (1981).

Lorenc, A., "A global three-dimensional multivariate statistical interpolation scheme," *Mon. Wea. Rev.* **109**, 701-721 (1981).

Luther, D., D. Harrison, and R. Knox, "Zonal winds in the central equatorial Pacific and El Niño," *Science* **222**, 327-330 (1983).

Machenhauer, B., "On the dynamics of gravity oscillations in a shallow water model, with application to normal mode initializations," *Contrib. Atmos. Phys.* **50**, 253-271 (1977).

Mangum, L., S. Hayes, and L. Stratton, "Sampling requirements for the surface wind field over the tropical Pacific Ocean," *J. Atmos. Ocean. Tech.* **9**, 668-679 (1992).

Masumoto, Y. and T. Yamagata, "On the origin of a model ENSO in the western Pacific," *J. Meteor. Soc. Japan* **69**, 197-206 (1991).

McCreary, J. and D. Anderson, "An overview of coupled ocean-atmosphere models of El Niño and the Southern Oscillation," *J. Geophys. Res.* **96**, 3125-3150 (1991).

McPhaden, M., H. Freitag, S. Hayes, and B. Taft, "The response of the equatorial Pacific Ocean to a westerly wind burst in May 1986," *J. Geophys. Res.* **93**, 10589-10603 (1988).

Morrissey, M. L., "An evaluation of ship data in the equatorial western Pacific," *J. Clim.* **3**, 99-112 (1990).

Newmann, C. and M. Lawrence, "An operational experiment in the statistical-dynamical prediction of tropical cyclone motion," *Mon. Wea. Rev.* **103**, 665-673 (1975).

Ogura, Y. and H. Chin, "A case study of cross-equatorial twin vortices over the Pacific in the northern winter using FGGE data," *J. Meteor. Soc. Japan* **65**, 669-674 (1987).

Philander, S. G., *El Niño, La Nina, and the Southern Oscillation,* (Academic Press, Inc., San Diego, CA, 1990).

Phoebus, P. and J. Goerss, "The assimilation of marine surface data into the Navy Operational Global Atmospheric Prediction System," *J. Marine Tech. Soc.* **26**, 63-76 (1992).

Ramage, C. S., "El Niño," *Science* **254**, 76-83 (1986).

Rasmusson E., and T. Carpenter, "Variations in tropical sea surface temperatures and surface wind fields associated with the Southern Oscillation/El Niño," *Mon. Wea. Rev.* **110**, 354-384 (1982).

Revell, C. and S. Goulter, "South Pacific tropical cyclones and the Southern Oscillation," *Mon. Wea. Rev.* **114**, 1138-1145 (1986).

Reynolds, R., K. Arpe, C. Gordon, S. Hayes, A. Leetma, and M. McPhaden, "A comparison of tropical Pacific surface wind analyses," *J. Clim.* **2**, 105-111 (1989).

Riehl, H.,*Tropical Meteorology*, (McGraw-Hill Book Company Inc., New York, NY, 1955).

Ropelewski, C. and T. Smith, "The evolution of the Southern Oscillation in the ocean and atmosphere from 1990 to 1992," Proceedings of the AMS Fourth Conference on Southern Hemisphere Meteorology and Oceanography, American Meteorological Society, Hobart, Australia, March 1993, 351-352.

Rosmond, T., "The design and testing of the Navy Operational Global Atmospheric Prediction System," *Wea. and Forecasting* **7**, 262-272 (1992).

Solow, A. and N. Nicholls, "The relationship between the Southern Oscillation and tropical cyclone frequency in the Australian region," *J. Clim.* **3**, 1097-1101 (1990).

Sui, C.-H., and K.-M. Lau, "Multiscale phenomena in the tropical atmosphere over the western Pacific," *Mon. Wea. Rev.* **120**, 407-430 (1992).

Wakata, Y. and E. Sarachik, "Unstable coupled atmosphere-ocean basin modes in the presence of a spatially varying basic state," *J. Atmos. Sci.* **48**, 2060-2077 (1991).

Xu, Y. and C. Neumann, "A statistical model for the prediction of western North Pacific tropical cyclone motion (WPCLPR)," NOAA Technical Memorandum NWS NHC 28, 1985. (Available from Environmental Science Information Center, EDS/NOAA, 3300 Whitehaven St. N.W., Washington, DC 20235.)